DESIGN AND CONTROL OF TELE OPERATED MOBILE PLATFORM

AMAREN PRASANNA DAS

DEPARTMENT OF MECHANICAL ENGINEERING
INDIAN INSTITUTE OF TECHNOLOGY DELHI
OCTOBER 2018

©Indian Institute of Technology Delhi (IITD), New Delhi, 2017

DESIGN AND CONTROL OF TELE OPERATED MOBILE PLATFORM

by

AMAREN P DAS

Department of Mechanical Engineering

Submitted

in fulfillment of the requirements of the degree of Doctor of Philosophy

to the

INDIAN INSTITUTE OF TECHNOLOGY DELHI

OCTOBER 2018

Certificate

This is to certify that the thesis entitled **DESIGN AND CONTROL OF TELE OPERATED MOBILE PLATFORM**, submitted by **Shri. Amaren Prasanna Das** to the Indian Institute of Technology Delhi, for the award of the degree of **Doctor of Philosophy** in Mechanical Engineering, is a record of the original, bona-fide research work carried out by him under my supervision and guidance. The thesis has reached the standards fulfilling the requirements of the regulations related to the award of the degree.

The results contained in this thesis have not been submitted in part or in full to any other university or institute for the award of any degree or diploma.

Dr. S. K. Saha
Professor
Department of Mechanical Engineering
Indian Institute of Technology Delhi
New Delhi - 110016, India

Acknowledgements

Amaren P Das

Abstract

XXXXXXXX xx xxxxxxxxxxx XXXX

Contents

Certificate i

Acknowledgements iii

Abstract iv

List of Figures vii

List of Tables xi

Important Symbols and Abbreviations xiii

1 Introduction **1**

1.1 Research Contributions 2

1.2 Thesis Organization 3

2 Literature Review **7**

2.1 Research Objectives 7

2.2 Summary 7

3 Design of Mobile Platform **9**

3.1 Design Overview 9

3.2 Design of the Traction System 11

3.2.1 Selection of Motor and Gearbox 13

3.3 Design of Steering System 14

3.3.1 Minimum Turning Radius 15

3.3.2 Calculation of Steering Torque 16

3.4 Design of Scissor Mechanism for Manipulating Arm 17

3.5 Summary 19

4 Dynamics of Wheeled Mobile Robots **21**

4.1 Modelling using the Natural Orthogonal Compliment (NOC) 22

4.2 Dynamic Equation of WMR 25

4.2.1 Kinematic analysis 26

4.2.2 Dynamic equations 30

4.2.2.1 Generalized Inertia Matrix, I 30

4.2.2.2 Matrix of Convective Inertia term C 31

4.3 Special cases 33

4.3.1 Standard caster ($d_1 = 0$) 33

4.3.2 Under Actuated Case ($d_2 = 0$) 33

4.4 Simulation 34

4.4.1 Inverse Dynamics 35

4.5 Summary 37

5 Control of mobile manipulator **39**

5.1 Control Architecture and Hardware 39

5.1.1 Local Onboard Controller 40

5.1.2 Details of Motor Controller 42

5.1.3 The control algorithm for platform 45

5.1.3.1 Wheel odometry 48

5.1.3.2 Control of Z platform 49

5.1.4 The Remote Control Station 51

5.2 Summary 51

6 Simulation Time Delay Tele-operation **53**

6.1 Modeling of mobile platform 54

6.2 Modeling the human operator 54

6.3 Simulation and Results 57

6.3.1 The Simulation Algorithm 57

6.4 Summary 60

7 Predictive Display **61**

7.1 Remote Scene Extrapolation 61

7.1.1 here 61

8 Conclusions **63**

8.1 Thesis Summary 63

8.2 Future Scope of the work 63

Bibliography **64**

A Simulation Time Delay Tele-operation **69**

A.1 Measurment of Time Delay in Video Feedback 69

B Dynamics **71**

B.1 Inertia Dyad 71

Publications from the Thesis 73

Brief Bio-data of the Author 75

List of Figures

3.1 3-D Model of the mobile manipulator 10
3.2 Photograph of the actual System 10
3.3 Rear Suspension 13
3.4 Mobile Manipulator on slope 13
3.5 Ackerman Steering Condition 15
3.6 Davis Steering Gear 16
3.7 Steer Torque 16
3.8 Scissor Mechanism 18

4.1 WMR-Std. Castor 25
4.2 WMR-general 25
4.3 Castor wheel configuration of a WMR 25
4.4 Path Traced by Robot 34
4.5 Inverse dynamics of the mobile robot 36

5.1 Control Architecture Block Diagram 39
5.2 Data sent from PC to Onboard controller 40
5.3 Wiring Diagram of Robot 41
5.4 EPOS4 Controller Block Digram 42
5.5 Current control bolck digram 42
5.6 Velocity control bolck digram 44
5.7 Position control bolck digram 44
5.8 provide suitable title 46
5.9 Tracing a line 49

5.10 Motor torque 49
5.11 Linear Velocity 49
5.12 Angular Velocity 49
5.13 Linear motion of WMR 49
5.14 Tracing a Circle 50
5.15 Motor torque 50
5.16 Linear Velocity 50
5.17 Angular Velocity 50
5.18 Circular motion of WMR 50
5.19 User Interface for teleoperation 51

6.1 Teleoperation Architecture 53
6.2 Assumed driving strategy 55
6.3 Geometry of Pure Pursuit 56
6.4 Teleoperation block diagram 58
6.5 Simulation with no time delay in either direction 59
6.6 Simulation with time delay $h_1 = .5sec$ and $h_2 = 0$ 59
6.7 Simulation with time delay $h_1 = .8sec$ and $h_2 = 0$ 60

List of Tables

3.1 Key parameters and specifications of the mobile manipulator. . . . 10

4.1 Dynamic & kinematic parameters 36

5.1 Proportionality constant table 41
5.2 Rear Right Motor Controller parameters 43
5.3 Rear Right Motor Controller parameters 43
5.4 Rear Steer Motor Controller parameters 45

Important Symbols and Abbreviations

The important conventions, symbols and abbreviations used in this thesis are listed in the alphabetical order.

Conventions	**Description**
italic	Scalar quantities in lower-case lightface italic with Latin/Greek letters
bold	Vectors are in lower-case boldface Latin/Greek letters
CAPITAL BOLD	Matrices are in upper-case boldface Latin/Greek letters

Latin letters	**Description**
$\mathbf{A}_t$	State transition matrix at time t
a_i, α_i b_i, θ_i	Represents four DH parameters namely, Link length, twist angle, joint offset and joint angle, respectively.
$\mathbf{B}_t$	Control input matrix at time t
$\mathbf{C}$, $\mathbf{C}_i$	Matrix of Convective Inertia (MCI) terms associated with the complete system and the i^{th} subsystem, respectively
f_v	Viscous friction coefficient at the joint of robotic manipulator
f_c	Coulomb friction coefficient at the joint of robotic manipulator
$\mathbf{x}$, $\hat{\mathbf{x}}_{t\|t-1}$	State vector and its estimate at time t with data upto time $(t-1)$
$\mathbf{0}$	Column vector of zeros or null vector with compatible size to the dimensions of the matrices and vectors where it appears
$\mathbf{1}$	Identity matrix of size compatible to the dimensions of the matrices where it appears

Greek letters	Description
α_i	Twist angle of k^{th} link (DH parameter)
θ_i, $\dot{\theta}_i$, $\ddot{\theta}_i$	Relative joint displacement of the i^{th} link, its rate, and acceleration, respectively, in a closed-loop system
$\boldsymbol{\theta}_i$, $\dot{\boldsymbol{\theta}}_i$, $\ddot{\boldsymbol{\theta}}_i$	Vector of relative joint displacement of the i^{th} link, its rate, and acceleration, respectively, in a closed-loop system
$\boldsymbol{\chi}_b$	Vector of base parameters in dynamic model
$\boldsymbol{\lambda}$	Lagrange multiplier representing constraint forces
$\boldsymbol{\omega}_i$	The 3-dimensional angular velocity vector of i^{th} link

Acronyms	
AMM	Aruco Marker Map
ANOVA	Analysis of Variance
VTM	Velocity Transformation Matrix

Functions/Operators	
$\kappa(\mathbf{M})$	Condition number of matrix $\mathbf{M}$
$det(\mathbf{M})$	Determinant of matrix $\mathbf{M}$
$diag(\mathbf{v})$	Element of vector $\mathbf{v}$ at diagonal position of a matrix

Chapter 1

Introduction

The use of robots such as robotic arm has been used in factories for a long time, basically for repetitive kind of job. Though it started with the intention to reduce human labour, production cost and increased productivity. With development of technology , their scope has expanded beyond manufacturing domain. Robots are now being used for health care, surveillance, exploration etc. The reduction in development cost of robotic system has resulted in introduction of robotic system in entertainment industries and personal care. Robots have matured form heavy duty serial linked mechanical arms to a more presentable form such as ASIMO by Haonda and Aibo by Sony.

In areas where human access is not preferred or restricted due to risk of life or inhospitable environmental conditions such as which exists in chemical, space or nuclear industries, robotic systems have gained huge popularity in providing services as surveillance, rescue, exploration & remote maintenance. Research in teleoperated and autonomous mobile robotics has been fuelled largely by these requirement. Teleoperated mobile robots are suitable for these applications as the work space required to be covered is very large and it is essential to maintain physical separation between the robot and its control station, moreover the remote environment is in general unknown.

This research too was motivated by a similar requirement for in-situ measurement of the radioactive radiation, mostly neutron field, inside the vault and cave areas of K-130, K-500 and Medical Cyclotron operational at VECC, Kolkata, West Bengal. Cyclotrons are used to accelerate charged particle beam to high energy. These are required for experiments in nuclear physics and nuclear medicine. The particles are accelerated to high energy using a high frequency alternating voltage which is applied between two hollow "D"-shaped sheet metal electrodes called "Dees" inside a vacuum chamber. The area surrounding the Dee is called the vault and cave is the areas where beam line (beam of accelerated particles) is available for experimentation. Radiation mapping of these areas are mandatory requirements for getting safety clearance from regulators during commissioning of new units and at regular intervals during operational life of the cyclotron facility. Though there are radiation detectors placed at different locations in these area they can only measure radiation levels at discrete location but can not provide the 3-D radiation map. The advantage of having a radiation map is that it provide detailed input to health physicist of the dose a person may receive and accordingly plan emergency operations. These maps also provide the plant operators with the location of radiation leakage and accordingly tune there system to improve its efficiency.

The challenge faced for in-situ inspection during operation of cyclotron is that the interaction between an accelerated beam of charged particles and the target produce Bremsstraghlung and characteristic x-rays, prompt γ-rays, neutrons and delayed radiation (β and γ) thus making human presence unacceptable. A tele-operated mobile robot with wireless communication link is the obvious solution. This thesis discusses design analysis and develop of a prototype robot to carry out in-situ measurement and mapping of radiation level.

1.1 Research Contributions

The original contributions of the present research are listed below:

(i) Design of customized teleoperated mobile robot for remote surveillance and mapping application.

(ii) Development of kinematic and dynamic model of the robot at hand.

(iii) Control architecture required for intuitive teleoperation of this mobile robot.

(iv) Predictive visual feedback control to alleviate problem arising due to time delayed.

1.2 Thesis Organization

The thesis contains eight chapters and one appendix. They are organized as follows:

Chapter 1: Introduction

The present chapter, discusses the scope of mobile robotics in general and the motivation which lead to this research followed by the organization of the thesis.

Chapter 2: Literature Review

This chapter presents the literature review in the following areas *kinematics and dynamics* of mobile robot, *control of mobile robot*, *control for time delay systems*, *performance of operator under teleopreration* and *predictive display systems.*

Chapter 3: Design of Mobile Platform

This chapter highlights the design considerations of tele-operated mobile platform based on environmental conditions mission requirements. This paper presents the design and control scheme of a mobile manipulator used for radiation survey of Cyclotron vault and cave regions. It discusses the mechanical design for the traction system, the steering gear and the scissor mechanism. Selection of steering system based on terrain condition and power requirement is also discussed.

Chapter 4: Mathematica Modelling of Wheeled Mobile Platform

In this chapter, we present the orthogonal compliment method for deriving the dynamic equation of four wheeled differentially driven platform. The platform has two actuated wheels and two passive wheels. Different types of passive wheels has been studied and there corresponding dynamic equation are presented. The main contribution of this paper is derivation of dynamic equation a differentially driven mobile platform with the most general form of passive wheel.

Chapter 5:Control of mobile manipulator

The control architecture and the hardware used for tele-operation is presented along with the detailed description of implementation of the controller software at both the remote (mobile robot) and the local station. The experimental results of robots position based on wheel odometry and is torque requirement for few predefined paths is presented. A comparison study with the simulated results based on dynamic analysis presented in chapter 4 is also presented.

Chapter 6: Simulation Time Delay Tele-operation

In this chapter simulation of a teleoperated mobile platform is presented both under time delay due to communication link and without time delay. It is shown via simulation that with increase in time delay the stability of the teleoperation loop become unstable. A mathematical model of human driver is also presented to simulate the human factor in the teleoperation loop.

Chapter 7: Predictive Display

In this chapter we propose a Predictive Display strategy to counter the time delay in video feedback by extrapolating in time the camera view based on the predicted position of the robot at remote location.

Chapter 8: Conclusions

This chapter summarizes major results of this research work. Limitations along with the future scope from the present experiences are also addressed.

Bibliography

Appendix A: Measurement of Time Delay in Video Feedback

Here the experimental set up and methodology used to determine the time delay is presented. In this appendix,

Chapter 2

Literature Review

This chapter presents the survey of the literature highlighting design of different mobile robots and there control either used for field operation or for academic research test platforms.

2.1 Research Objectives

Based on the surveyed literature the objective of the present research are listed below:

- Identify
- To
- To
- Deve
- Es
- To

2.2 Summary

This chapter provided the

Chapter 3

Design of Mobile Platform

Most of the mobile robots presented in literature uses differential wheel drive with passive castor, as in [1], [2] and [3]. The other common methods for locomotion of mobile robots are the omnidirectional wheels [4] and [5], and tracked wheel system [6] and [7]. According to Nagatani [8], a vehicle with Mecanum wheels is susceptible to slippage and same is the case for tracked vehicle, which are inherently skid steered. The slippage of the wheels prevents the most popular dead-reckoning method using rotary shaft encoders from being performed well. This chapter discusses the design methodology of a novel mobile manipulator based on environmental requirements. We also highlight the advantage of the Davis steering mechanism over castor wheels or other steering methods from the perspective of this mobile manipulator. The Davis steering system modifies the heading of front wheels in a way that, at low speeds, all the wheels are in pure rolling without lateral sliding [9].

3.1 Design Overview

The objective of a mobile robot under consideration is to navigate inside the cyclotron vault and collect radiation intensity data at all the required points decided by the operator. Data is to be collected not only at different planer locations of the floor but also at varying height from the floor. To cater to this operational

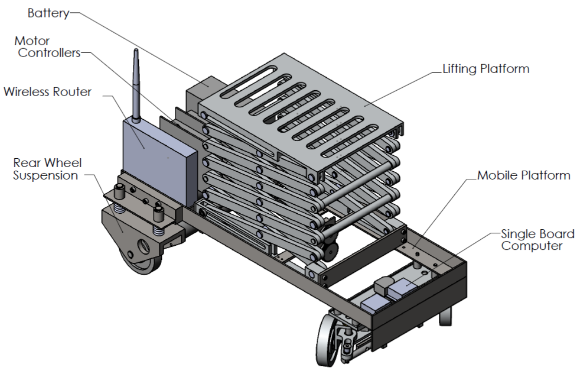

Figure 3.1: 3-D Model of the mobile manipulator

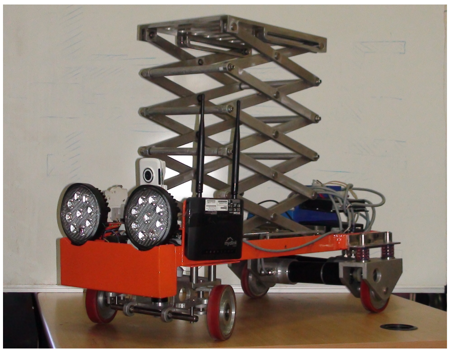

Figure 3.2: Photograph of the actual System

requirement, a mobile platform with a vertically extendable manipulating arm was developed as shown in Figures 3.1 and 3.2. Together, they are referred henceforth as mobile-manipulator. The 3-D model of the mobile-manipulator with its major subsystems are shown in Figure 3.1, whereas and the actual system is shown in Figure 3.2.

The environmental condition required that the vehicle be either autonomous or teleoperated. To keep the complexity low it was decided to have wireless teleoperated navigation and control. This gives an operator full flexibility to drive and control the system from a remote station using visual feedback provided by the on board camera. The key parameters of the mobile manipulator are listed in Table 3.1.

Table 3.1: Key parameters and specifications of the mobile manipulator.

Weight	70 Kg	without payload
Payload	10 Kg	—
Footprint	700 mm × 400 mm	-
Height Collapsed	500 mm	Along Z-Axis
Height Extended	1500 mm	Along Z-Axis
Steering mechanism	Davis Steering	–
Turning radius	415 mm	-
Ground clarence	45 mm	–
Maximum traction speed	2 m/min	On flat terrain
Ramp climb angle	30°	Checkerboard surface

The mobile-manipulator has a footprint of 700 mm x 400 mm based on the narrow passage through which the system has to negotiate. These passages are formed inside the vault area by the pipelines and structural supports of the cyclotron and its associated equipment. Two DC motors,with speed servo controller, provide the traction to each rear wheels. The two front wheels are inter-connected with a Davis steering mechanism [10]. A scissor mechanism provides the vertical motion of the detector that is mounted on the manipulating arm.

In order to keep the self weight of the system small all the structural parts are made of aluminum alloy AL6061, apart from the base frame. Stainless Steel (SS304) angle sections was used for the base frame, which give it excellent strength to weight ratio.

3.2 Design of the Traction System

Traction is provided by the two rear wheels driven independently. This makes the system over actuated. A mechanical differential connecting the two rear wheels, as used in cars, would overcome this. It was not proposed to do so as the proposed vehicle is planned to be teleoperated in a environment inaccessible to humans. This calls for a single-failure-safe design. The proposed design gives two major advantages. Firstly, in case one of the wheel loosing contact with the ground due to overhang in small pits or while over an obstacle, the mechanical differential system would keep supplying power to the free hanging wheel. The system will hence get stuck, maybe in an unrecoverable location. This situation is avoided in the present design as the motor having traction can be independently powered, to move the vehicle. Secondly, using the proposed design, in case of one actuator failure, either the traction or the steering motor, still the vehicle can be manoeuvred to a safe location, albeit with dragging of the wheel with failed actuator.

Each wheel is driven by a Maxon DC RE50 200W Motor through a 26:1 reduction gearbox. The motors are mounted at an offset to the wheel axis for increased ground clearance, as shown in Figure 3.3. Spring suspension is provided at each wheel to ensure sufficient contact force on uneven ground. The diameter of the wheel is 100 mm (D_w), which is sufficient to ride over obstacle of height 20 mm (Max). They are made of Aluminum alloy-6061 with 5mm thick molded polyurethane (PU) liner. The PU liner provides large traction on cement flooring while being resistance to wear.

The load distribution was optimized to generate maximum normal reaction, F_n, at the rear wheels without overturning while moving up the ramp of 30^o. Maximizing rear wheel reaction by increasing "b" as per Equation 3.1 ensures increased traction, $F_T = \mu F_N$ (μ is the coefficient of friction), but at the same time decreases the stability margin indicated by "X" in Figure 3.4. The static moment and force balance yield

$$F_{N2} = \frac{b}{a} F_{N1}, \quad F_{N1} + F_{N2} = mg \cos\theta \tag{3.1}$$

The stability margin X as shoen in Figure 3.2 was fixed as $30mm$ so as to achieve maximum acceleration of $0.144g$ over the ramp of 30^o without overturning. This was done based on the condition of dynamic stability given by

$$mgb \cos\theta = (mg \sin\theta + ma) z_{cg}, \quad \Rightarrow g(\frac{b}{z_{cg}} \cos\theta - \sin\theta) = a \tag{3.2}$$

Where

F_{N1}, F_{N2} are normal reaction on the front and rear wheels.

a and b are the distance of the vehicle cg from the rear and front wheels.

Z_{cg} is the height of the cg from the plane containing the contact point of the wheels.

m is mass of the vehicle.

g is acceleration due to gravity.

θ is the inclination of the traction surface from horizontal.

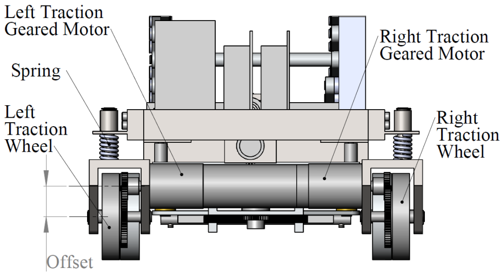
Left Traction Geared Motor
Spring
Left Traction Wheel
Offset
Right Traction Geared Motor
Right Traction Wheel

Figure 3.3: Rear Suspension

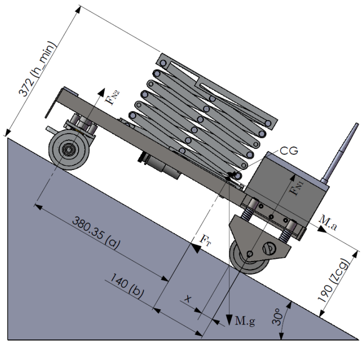
372 (h_min)
F_{N2}
CG
F_{N1}
M.a
380.35 (a)
F_T
140 (b)
x
M.g
30°
190 (Zcg)

Figure 3.4: Mobile Manipulator on slope

3.2.1 Selection of Motor and Gearbox

The torque requirement for each rear wheel was calculated based on the static moment balance with the assumption that each rear wheel shares equal load and the total suspended weight is 80 Kg. From the freebody diagram (Figure 3.4), using moment and force balance we get the following:

$$F_{N1} = \frac{aM\cos\theta}{a+b-\mu Z_{cg}}, \qquad F_T = \mu F_{N1} \tag{3.3}$$

In order to estimate the traction motor size, we take worst case scenario of $\theta = 30^o$ and $\mu = 0.3$. This leads to

$$F_{N1} = 66Kg, \qquad F_T = 0.3 * 66 \approx 20Kg$$

Since the traction is provided by the two rear wheels, the torque required per wheel (T_w) is given by

$$T_w = (F_T/2)(D_w/2) = (20/2) * 50 = 500Kg - mm \simeq 5Nm \tag{3.4}$$

The motor torque T_M, required based on the assumption of factor of safety, $FS =$ 1.5 is

$$T_M = (FS) * T_w = 1.5 * 5 = 7.5 \simeq 8Nm \tag{3.5}$$

Assuming the maximum speed, $V_{ramp} = 1m/s$, of the mobile manipulator over a ramp, the required power, P_M, of the traction motor is calculated as,

$$\begin{aligned} \omega_w &= V_{ramp}/(D_w/2) \simeq 200rpm \\ P_m &= \omega_w T_m = 20 * 8 = 160W \end{aligned} \tag{3.6}$$

The nearest Maxon motor available as per the catalogue [11] is 200W, RE50-370354 motor. The nominal speed, N_s is 5680rpm. Therefore, the gearing ratio required is, $N_s/\omega_w = 5680/200 \simeq 28.4$. The nearest gear box available is of ratio 26 : 1, which was chosen.

3.3 Design of Steering System

The design objective of a steering system should ensure rolling motion of all the wheels during every possible manurers of the mobile robot. This is important to reduce the friction drag due to sliding motion which reduces the energy efficiency of the mobile robot. In case of four wheeled vehicle with rear wheels fixed and front wheels steered the condition is shown in Figure 3.5, referred in some literature as Ackerman steering conduction.

This mobile manipulator uses Davis steering mechanism, Figure 3.6, on the front wheels. Caster wheels were not used as they tend to align with obstacles and thus get stuck. On the other hand tracked wheels have excellent rough terrain capabilities, but is power intensive due to skid steering. another option was to use Omnidirectional wheels, which need complex controller for coordination and an extra actuator. Moreover, the operation are are in general not clean of loose small objects, which may get stuck in between the free rollers of the omnidirectional wheels. This will reduce the efficiency of the vehicle.

Davis mechanism was chosen over Ackerman steering gear as it satisfies the steering condition given by Equation 3.7, which ensures pure rolling of all wheels over the entire steering range. This makes the system suitable for passive wheel

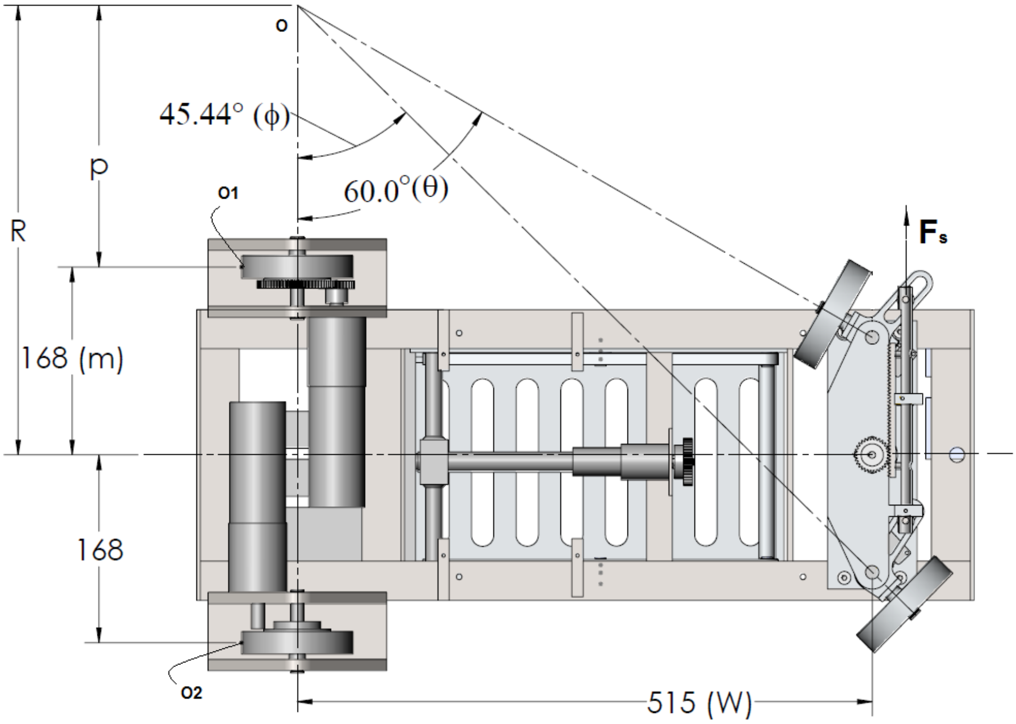

Figure 3.5: Ackerman Steering Condition

odometry and energy efficient. The mechanism being positively driven by position controlled servo motor does not align with the obstacles and thus are able to crossover it. The dimensions of the links used in the steering mechanism is given in Figure 3.6, and are based on the Ackerman steering law given below:

$$\cot\phi - \cot\theta = a/w, \quad \frac{2b}{h} = \frac{a}{w} \tag{3.7}$$

Where a and b is limited by the over all size of the vehicle, discussed earlier.

3.3.1 Minimum Turning Radius

The mechanical construction of this steering mechanism limits the steering angle. This in turn limits the minimum radius the vehicle can negotiate. Figure 3.5 shows the extreme values of ϕ and θ, one side of the steering limits. The **turning radius** R for a given steer angle θ is calculated by the geometry of Figure 3.6 as

$$\tan\theta = \frac{w}{P + m - \frac{a}{2}} \quad \text{and} \quad R = m + p$$

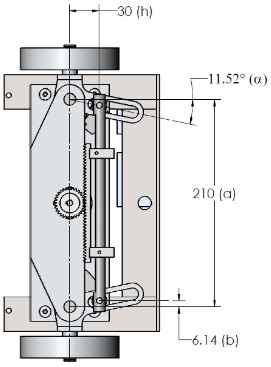

Figure 3.6: Davis Steering Gear

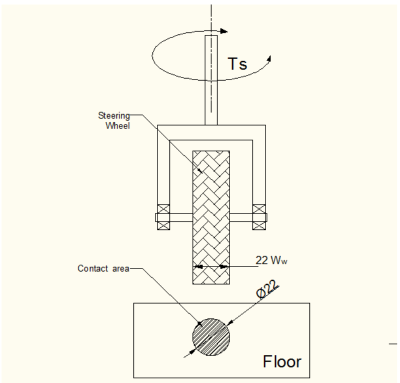

Figure 3.7: Steer Torque

Substituting R and rearranging the above equation, we get

$$R(\theta) = \frac{a}{2} + w \cot \theta \tag{3.8}$$

The extreme value of $\theta = 60$. as shown in Figure 3.5, this gives the *minimum turning radius* R_{min} as

$$R_{min} = \frac{210}{2} + 515 \times cot(60^o) = 402mm$$

3.3.2 Calculation of Steering Torque

The torque required to steer the front wheel is estimated based on a simplified assumption that the wheel deforms under normal load and the contact area thus generated is circular in shape with diameter that of the wheel width, W_w, as shown in Figure 3.7. In order to estimate the normal reaction on each wheel, we assume that the total weight of 80kg is equally shared by the four wheels. Therefore, $N_s = 80/4 = 20Kg$. Next, the uniform pressure formula used for brakes/clutches design was applied to find the resistance torque T_s, between the ground and the wheel i.e,

$$T_s = \frac{N_s \mu}{3} W_w = 0.4Nm \tag{3.9}$$

The resistance torque, T_s, of both the wheels are balanced by the force F_s acting on the rack as shown in Figure 3.6. The rack is coupled to the steering motor by a pinion of diameter, $D_p = 40mm$. The motor torque, T_{m_s} in Equation 3.10 is calculated with a high factor of safety, $FS = 3$. This is because T_S is estimated based on a simplified model of brake design. The power, P_{m_s} of the steering motor based on torque T_{m_s} and the steering speed ω_s of 100rpm is

$$T_{m_s} = (FS)\frac{2T_s}{h}\frac{D_p}{2} = 1.6Nm \quad \text{and} \quad P_{m_s} = T_{m_s} * \omega_s = 17W \tag{3.10}$$

Based on the above specifications, a 20W, RE25 DC motor of Maxon make and a gear box GP32 of ratio 159:1 was chosen for the steering mechanism.

3.4 Design of Scissor Mechanism for Manipulating Arm

The manipulating arm was designed to move up to a height of 1.5m from the floor level. This motion was generated using a scissor mechanism, as shown in Figure 3.8. The scissor mechanism has two major advantages over other lifting methods such as telescopic pillar, etc. First, the ratio of height in extended and collapsed condition is very large. In our case it is $3 : 1$. Second, the self weight of the mechanism is less as it is made of rectangular links.

The scissor mechanism, Figure 3.8, has 6 stages, where one "X" denotes one stage. The Scissor is connected to the top platform by a pivot joint O_2 and a prismatic joint A_2. This is coupled to the base frame by pivot joint O_1 and a prismatic joint A_1. The linear actuation of joint A_1 is provided by a lead screw of pitch (P) 1.5 mm and mean diameter (d_m) 10mm. This results in vertical motion of the top platform.

The relation between the vertical motion of the platform and the horizontal displacement of point $A_!$ is given by geometry of the mechanism shown in Figure

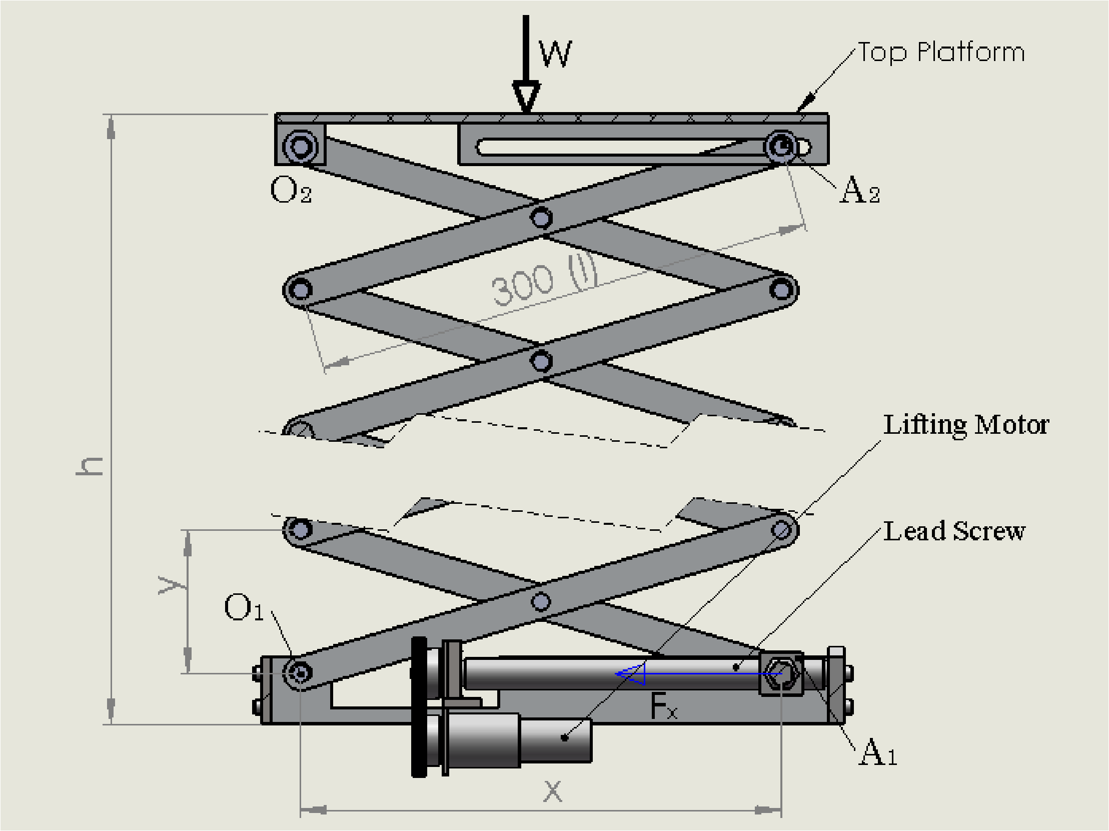

Figure 3.8: Scissor Mechanism

3.8

$$\begin{aligned} & y = l\sin\theta,\ x = l\cos\theta,\ \Rightarrow dy = l\cos\theta d\theta,\ dx = -l\sin\theta d\theta \\ & h = Ny \rightarrow dh = Ndy \end{aligned} \tag{3.11}$$

where l is the link length, θ the angle of the link with horizontal plane and h the height of platform.

The number of stages used in the scissor mechanism is N=6. From the principle of virtual work, we get

$$-F_x dx = W dh,\ \Rightarrow F_x = \frac{WN}{\tan\theta} \tag{3.12}$$

where, F_x is the axial force on the prismatic joint, A_1 and W is the payload. From Equation 3.12, it is clear that as $\theta \rightarrow 0$, the force $F_x \rightarrow \infty$. In the present design, $\theta_{min} = 5^o$ and $\theta_{max} = 45^o$. Therefore, the extended height $h_{max} = Nl\sin\theta_{max} = 1.3m$ and the collapsed height $h_{min} = 156mm$. Assuming $W = 8kg$ as payload the maximum force $F_x = 342Kg$ is required at $\theta_{min} = 5^o$, .

The motor torque required for the scissor mechanism is calsulated using screw jack formula given in [10] and here presented as Equation 3.13.

$$T_L = \frac{F_x d_m}{2}\left(\frac{p + \pi \mu d_m \sec\alpha}{\pi d_m - \mu p \sec\alpha}\right) = 7.5Nm \tag{3.13}$$

where coefficient of friction assumed, $\mu = 0.1$, ACME thread angle $2\alpha = 60^o$, pitch diameter $d_m = 15mm$ and pitch $p = 1.5mm$ is used. Based on the above specification 10W RE20 DC motor with a gear box of 25:1 ratio was chosen from Maxon motor catalogue [11].

3.5 Summary

Design calculations for the proposed mobile manipulator are presented in this chapter. Different aspects based on the requirements of radiation inspection around cyclotron was taken into account. Advantage of positively steered wheels over caster wheel was highlighted for the proposed mobile robot.

Chapter 4

Dynamics of Wheeled Mobile Robots

In the field of mobile robotics, extensive research has been carried out. Mobile robots can broadly be divided into three categorises-wheeled robots, legged robots [12], and aerial vehicles [13]. There are few mobile robots which use both wheels and legs for locomotion for example, in Creadapt [14] in order to take advantage of both modes of locomotion. Among these the most extensively studied are the Wheeled Mobile Robots (WMR). They have been classified into five generic classes by Champion etal. [15], [16] based on there mobility resulting from the kinematic constrains due to different wheel types. The most common among these are the 3 wheeled differential drive WMR with one castor wheel. Because of its simplicity in modelling, they have been used in most of the control and motion planing algorithms [17], [18] and [19].

In order to develop a model-based control algorithm it is imperative to have good dynamic model of the WMR. These dynamic models are used in simulation software, Software in Loop (SIL) testing and Hardware in Loop (HIL) testing of the controllers. Different methods have been adopted to derive the dynamic model of WMRs. A general dynamical model was derived for three-wheel mobile robots with nonholonomic constraints by B. d'Andrea-Novel [20] using Lagrange formulation. Alternatively Thanjavur and Rajagopalan [21] has used Kane's method and Saha et al. [22],[3] used Natural Orthogonal Compliment (NOC) method for the same.

All the papers known to us use the standard caster wheel in deriving the dynamic model of the WMR. In this chapter the modelling is carried out considering the Castor wheel in the most general configuration. In the stranded castor wheel configuration the axis of rotation is perpendicular to the line joining the pivot and the axis of rotation, as shown in Figure 4.1 whereas in this study they are oriented in the most general way, as shown in figure Figure 4.2. The concept of the NOC which here inherently takes into account the non-holonomic constraint of the wheels has been used. Moreover, being a matrix based approach, it is convenient for numerical simulations.

4.1 Modelling using the Natural Orthogonal Compliment (NOC)

Let us consider a system n rigid bodies interconnected with different types of joints. Let f_i be the net force acting at the center of mass (CM) of the $i-th$ body and n_i is the net moment. If m_i is the mass, I_{ci} is the moment of inertia with respect to the CM, c_i is the position vector of the CM and ω_i is the angular velocity of the same body, then equation of motion of the $i-th$ rigid body is given by Newton-Euler equations as

$$f_i = m_i \ddot{c}_i \quad and \quad n_i = I_{ci}\omega_i + \omega_i \times I_{ci}\omega_i \tag{4.1}$$

Let us define twist (t) and wrench(w) as

$$t_i \equiv \begin{pmatrix} \omega_i \\ \dot{c}_i \end{pmatrix} \quad w_i \equiv \begin{pmatrix} n_i \\ f_i \end{pmatrix}$$

Note that the wrench w_i acting on the $i-th$ body can be decomposed into w_i^w, called the *working component* and w_i^C, the *non-working component*. The working component consists of all the external forces and torques, which imparts/extracts energy to/from the system, e.g. motor actuating torque. The non-working component of the wrench consists of the forces and torques that are used to constrain the motion of the body at the joints. Then, Newton-Euler equation (4.1) can be rewritten in a single matrix equation as

$$M_i\dot{t}_i + W_i M_i t_i = w_i^w + w_i^c \quad \because w_i \equiv w_i^w + w_i^c \tag{4.2}$$

where

$$M_i \equiv \begin{pmatrix} I_{ci} & 0 \\ 0 & m_i\tilde{1} \end{pmatrix}, \quad W_i \equiv \begin{pmatrix} \Omega_i & 0 \\ 0 & 0 \end{pmatrix}, \quad \Omega_i \equiv \omega_i \times \tilde{1} \tag{4.3}$$

in which $\omega_i \times 1$, is refered as the crossproduct matrix of vector ω_i and $\tilde{1}$ denotes the identity matrix. For details, refer to [23],[24].

If we define

$$M \equiv diag[M_1, M_2, ...M_n[, \quad W \equiv diag[W_1, W_2, ...W_n], \quad t \equiv [t_1^T, t_2^T, ...t_n^T]^T$$

and

$$w^j \equiv [{w_1^j}^T, {w_2^j}^T, ...{w_n^j}^T]^T, \, j = c, w$$

Then the equation of all the n rigid bodies in the system can be collected and written as a single matrix equation as

$$M\dot{t} + WMt = w^c + w^w \tag{4.4}$$

The above equation is referred to as decoupled equations of motion of the system.

The kinematic constraints both holonomic and non-holonomic (e.g. pure rolling) between two bodies i and j of a system can be expressed as linear homogeneous system of algebraic equations [23], namely

$$A_i t_i + A_j t_j = 0 \tag{4.5}$$

where A_i, A_j depend on the kinematic parameters.

The constraint equations corresponding to all the joints in the system can be written in terms of the *generalized twist vector* t. Furthermore if, $\dot{\theta} \equiv (\dot{\theta}_1, \dot{\theta}_2, ...)^T$ denote the *independent generalized joint rates*, one can then write t in terms of $\dot{\theta}$ as $t = T\dot{\theta}$. Using the fact, that $\dot{\theta}$ can take any arbitrary value, we get

$$At = 0, \quad \Rightarrow AT\dot{\theta} = 0 \quad \Rightarrow AT = 0 \tag{4.6}$$

The above equation (4.6) indicates that T is the orthogonal compliment of A. Since this relation arises naturally, hence the name *Natural Orthogonal Complement.* It can be shown [23] that the non-working wrench w^c lies in the range space of A^T. In view of equation 4.6, it can also be proved that w^c lies in the null space of T^T, therefore

$$T^T w^c = 0 \tag{4.7}$$

To eliminate the non-working forces and moments, i.e. w^C from the uncoupled equation of motion (4.4), we multiply both sides of the equation by T^T,

$$T^T M\dot{t} + T^T WMt = T^T w^W, \quad \Rightarrow T^T MT\ddot{\theta} + T^T(M\dot{T} + WMT)\dot{\theta} = T^T w^T \tag{4.8}$$

Equation 4.8 represents the dynamic equation of interconnected n-body system. This equation is expressed in terms of the independent generalized joint rates $\dot{\theta}$ and cosponsoring acceleration $\ddot{\theta}$. Further. using the relations $t = T\dot{\theta}$ and $\dot{t} = \dot{T}\dot{\theta} + T\ddot{\theta}$ in equation 4.8 the final equations of motion can be written as

$$I(\theta)\ddot{\theta} = C(\theta, \dot{\theta})\dot{\theta} + \tau \tag{4.9}$$

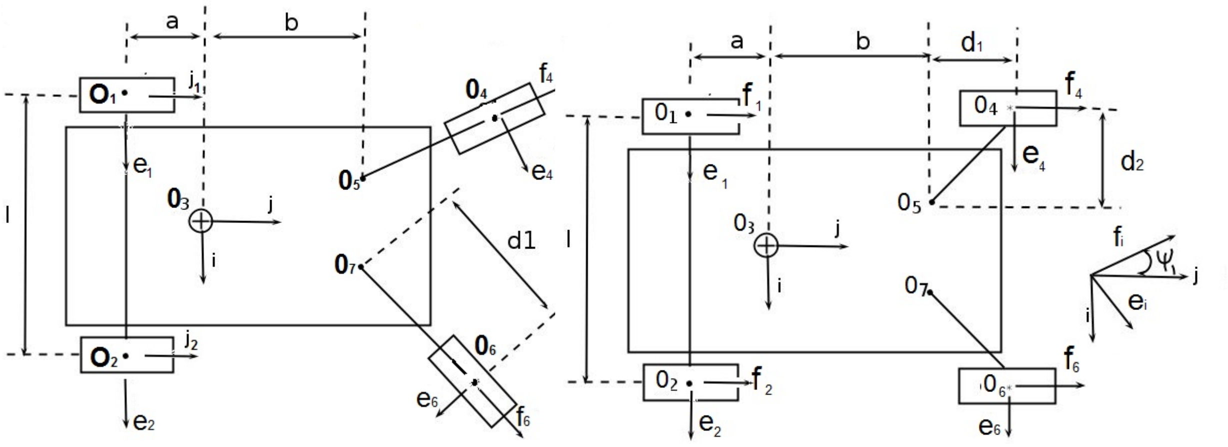

Figure 4.1: WMR-Std. Castor

Figure 4.2: WMR-general

Figure 4.3: Castor wheel configuration of a WMR

where

$$I(\theta) \equiv T^T M T \quad : \text{generalized inertia matrix}$$

$$C(\theta, \dot{\theta}) \equiv -T^T(M\dot{T} + WMT)\dot{\theta} \quad : \text{generalized matrix of convective inertia terms}$$

$$\tau \equiv T^T w^T \quad : \text{ generalized vector of driving forces}$$

4.2 Dynamic Equation of WMR

The dynamic equation of a differentially driven 3 wheeled mobile robot based on the Natural Orthogonal Compliment (NOC) has been presented by Saha [22]. The vehicle consisted of 2 driven wheel and one standard caster wheels. In general, for large vehicles, it necessary to have at least four wheels from the point of stability of the vehicle. Such a vehicle is shown in figure 4.1. It may be noted that the caster wheels used in this case are the standard caster wheel configuration, where the angle between line O_4O_5 and vector e_4 is 90 deg. Which is a special case of the more general configuration of the caster wheels shown in figure 4.2, where angle between line O_4O_5 and vector e_4 is not 90 deg

The vehicle considered for analysis in this chapter is shown in figure 4.2. It consists of two independently driven wheels at the back and two generalized caster wheels at the front. The actuated wheels are labelled as body #1 and #2. The platform is body #3. The first caster wheel and its bracket is labelled as #4 and #5 respectively, with the castor pivoted at O_5. Similarly the second castor is pivoted at O_7, and its bracket and wheel is labelled as #6 an #7 respectively, all the wheels are assumed to be rolling without slipping.

4.2.1 Kinematic analysis

In order to proceed with the kinematic analysis of the vehicle in figure 4.2, we define a orthogonal triad of vectors i, j, k at point O_3, the control point of the platform, as shown in the figure. If $\dot{\theta}_1$ and $\dot{\theta}_2$ [1] denote the rates of rotation of wheel #1 and #2 then the linear velocity of points O_1 & O_2 under pure rolling condition is given by

$$\dot{\boldsymbol{o}}_{\boldsymbol{i}} = r\dot{\theta}_i j, \quad \text{r=radius of wheel} \tag{4.10}$$

The angular velocity of the platform ω_3 can be written as

$$\boldsymbol{\omega_3} = (r/l)(\dot{\theta}_1 - \dot{\theta}_2)\boldsymbol{k} \tag{4.11}$$

Further, the velocity of point O_3 can be written as $\dot{\boldsymbol{o}}_{\boldsymbol{3}} = \dot{\boldsymbol{o}}_{\boldsymbol{i}} + \boldsymbol{\omega_3} \times (\boldsymbol{c} - \boldsymbol{o_i})$, $\quad i = 1, 2$. Where o_3 and o_i is the position vector of points O_3 and O_i respectively, with respect to some point fixed to the ground. By eliminate ω_3 we get the following:

$$\dot{\boldsymbol{o}}_{\boldsymbol{3}} = [(ar/l)(\dot{\theta}_1 - \dot{\theta}_2) + (r/2)(\dot{\theta}_1 + \dot{\theta}_2)]\boldsymbol{i} \tag{4.12}$$

Now, the angular velocity of the drive wheel #1 can be expressed as $\boldsymbol{\omega_1} = -\dot{\theta}_1 i + \omega_3 k$. Using equation 4.11, the same can be rewritten as

$$\boldsymbol{\omega_1} = \begin{pmatrix} -i + (r/l)k & -(r/l)k \end{pmatrix} \begin{pmatrix} \dot{\theta}_1 \\ \dot{\theta}_2 \end{pmatrix} \tag{4.13}$$

---

[1] positive when pointing along i

Based on equations 4.10 and 4.13, we can write the twist for wheel #1 in terms of $\dot{\theta}_a \equiv (\dot{\theta}_1, \dot{\theta}_2)^T$, as

$$t_1 = \begin{pmatrix} \omega_1 \\ \dot{o}_1 \end{pmatrix} = \begin{pmatrix} -i + (r/l)k & -(r/l)k \\ rj & 0 \end{pmatrix} \begin{pmatrix} \dot{\theta}_1 \\ \dot{\theta}_2 \end{pmatrix} \tag{4.14}$$

Similarly, for the other actuated wheel #2, one get

$$t_2 = \begin{pmatrix} \omega_1 \\ \dot{o}_1 \end{pmatrix} = \begin{pmatrix} -i + (r/l)k & -(r/l)k \\ 0 & rj \end{pmatrix} \begin{pmatrix} \dot{\theta}_1 \\ \dot{\theta}_2 \end{pmatrix} \tag{4.15}$$

To calculate the twist, t_3 of the platform body #3, equation 4.11 and 4.12 are combined to get

$$t_3 = \begin{pmatrix} \omega_3 \\ \dot{o}_3 \end{pmatrix} = \begin{pmatrix} \rho\delta & -\rho\delta \\ r(\lambda i + (1/2)j) & r(-\lambda i + (1/2)j) \end{pmatrix} \begin{pmatrix} \dot{\theta}_1 \\ \dot{\theta}_2 \end{pmatrix} \tag{4.16}$$

where

$$\delta \equiv d/l, \quad \rho \equiv r/d, \quad \lambda \equiv a/l$$

From the above three equations we get $T_1 = \begin{pmatrix} -i + (r/l)k & -(r/l)k \\ rj & 0 \end{pmatrix}$, $T_2 = \begin{pmatrix} -i + (r/l)k & -(r/l)k \\ 0 & rj \end{pmatrix}$, $T_3 = \begin{pmatrix} \rho\delta & -\rho\delta \\ r(\lambda i + (1/2))j & r(-\lambda i + (1/2))j \end{pmatrix}$

In order to calculate the twist of the caster bracket and the caster wheel, we need to express the unactuated joint rates, $\dot{\psi}_1$ and $\dot{\phi}_1$, in terms of the actuated joint rate vector $\dot{\theta}_a$. note here that $\dot{\psi}_1$ denotes the rate of rotation of bracket body #5 about O_5 with respect to the platform, and $\dot{\phi}_1$ the rate of rotation of caster wheel body #4 about its axis e_4 with respect to bracket. The velocity of O_5 can be expressed in two independent forms,namely, one in terms of the velocity of O_3 and the other one in terms of the velocity of O_5, i.e.,

$$\dot{o}_5 = \dot{o}_4 + \omega_5 \times (d_1 e_4 - d2 f_4), \quad \dot{o}_5 = \dot{o}_4 + \omega_5 \times (d_1 e_4 - d2 f_4) \tag{4.17}$$

On equating the above two equations together, and using the rotation matrix between coordiante system $\{i, j, k\}$ and $\{e_4, f_4, k\}$, to express the equation in e_4 and f_4, we get

$$(-\dot{\phi}_1 r + \dot{\psi}_1 d_1) f_3 + d_3 \dot{\psi}_1 e_3 = \dot{o}_3 + \omega_3 (m \cos\psi_1 - b \sin\psi_1 - d_1) e_4 \tag{4.18}$$

Taking the dot product of the above equation first with e_4 and then with f_4, and using equation 4.12 for $\dot{o}_3$, we get

$$\begin{aligned} \begin{pmatrix} d_2 & 0 \\ -d_1 & r \end{pmatrix} \begin{pmatrix} \dot{\psi}_1 \\ \dot{\phi}_1 \end{pmatrix} &= \begin{pmatrix} (-ar/l)S_{\psi_1} + (r/2)C_{\psi_1} + \delta_1 & (ar/l)S_{\psi_1} + (r/2)C_{\psi_1} - \delta_1 \\ (ar/l)C_{\psi_1} + (r/2)S_{\psi_1} + \delta_2 & (-ar/l)C_{\psi_1} + (r/2)S_{\psi_1} - \delta_2 \end{pmatrix} \dot{\theta}_a \\ &= [F_{ij}]\dot{\theta}_a \end{aligned} \tag{4.19}$$

where,

$$\delta_1 = (r/l)(mC_{\psi_1} - bS_{\psi_1} - d2, \quad \delta_2 = (r/l)(mS_{\psi_1} + bC_{\psi_1} + d_1)$$

Similarly, for the other caster wheel we get,

$$\begin{aligned} \begin{pmatrix} d_2 & 0 \\ -d_1 & r \end{pmatrix} \begin{pmatrix} \dot{\psi}_2 \\ \dot{\phi}_2 \end{pmatrix} &= \begin{pmatrix} (-ar/l)S_{\psi_2} + (r/2)C_{\psi_2} - \delta_3 & (ar/l)S_{\psi_2} + (r/2)C_{\psi_2} + \delta_3 \\ (ar/l)C_{\psi_2} + (r/2)S_{\psi_2} + \delta_4 & (-ar/l)C_{\psi_2} + (r/2)S_{\psi_2} - \delta_4 \end{pmatrix} \dot{\theta}_a \\ &= [G_{ij}]\dot{\theta}_a \end{aligned} \tag{4.20}$$

where,

$$\delta_3 = (r/l)(mC_{\psi_2} + bS_{\psi_2} + d2, \quad \delta_4 = (r/l)(mS_{\psi_2} + bC_{\psi_2} + d1$$

The angular and the liner velocity of the CM of the caster wheel,#4 is written in-terms of the co-ordinate frame fixed to the bracket #5, i.e. $\{e_4, f_4, k\}$, as

$$\omega_4 = \dot{\phi}_1 e_4 + (\omega_3 + \dot{\psi}_1)k, \quad \dot{o}_4 = \dot{\phi}_1 e_4 \tag{4.21}$$

Using equations 4.19 and 4.11, the twist t_4 can be written as

$$t_4 = \begin{pmatrix} \Theta_4 \\ C_4 \end{pmatrix} \dot{\theta_a} \tag{4.22}$$

Using the definition of $F(i,j)$ in equation 4.19, Θ_4 and C_4 can be written as

$$\Theta_4 = [F_{11}e_4 + \bar{F_{21}}k \quad F_{12}e_4 + \bar{F_{22}}k], \quad C_4 = r[-F_{11}f_4 \quad - F_{12}f_4]$$

$$\bar{F_{21}} = F_{21} + \rho\delta, \quad \bar{F_{22}} = F_{22} - \rho\delta$$

The angular and the liner velocity of the CM of the caster bracket#5 expressed in the co-ordinate frame fixed to the bracket is given by

$$\omega_4 = \dot{\phi_1}e_3 + \dot{\psi_1}k, \quad \dot{o_4} = \dot{o_4} + \omega_5 \times [-df_3] \tag{4.23}$$

Using equations 4.11 & 4.20, the twist t_5 can be written as

$$t_5 = \begin{pmatrix} \Theta_5 \\ C_5 \end{pmatrix} \dot{\theta_a} \tag{4.24}$$

where

$$\Theta_5 \equiv [\bar{F_{21}}k \quad \bar{F_{22}}k], \quad C_5 \equiv d[(1/2)\bar{F_{21}}e_4 - \rho F_{11}f_4 \quad (1/2)\bar{F_{22}}e_4 - \rho F_{12}f_4]$$

In a similar manner, the twist t_6 and t_7 of the other caster wheel and its bracket can be written as

$$t_6 = \begin{pmatrix} \Theta_6 \\ C_6 \end{pmatrix} \dot{\theta_a}, \quad t_7 = \begin{pmatrix} \Theta_7 \\ C7 \end{pmatrix} \dot{\theta_a} \tag{4.25}$$

Using $G(i,j)$ defined in equation 4.20, Θ_6, C_6, Θ_7 and C_7 can be written as

$$\Theta_6 \equiv [G_{11}e_6 + \bar{G_{21}}k \quad G_{12}e_6 + \bar{G_{22}}k], \quad C_6 \equiv r[-G_{11}f_6 \quad - G_{12}f_6]$$

$$\Theta_7 \equiv [\bar{G_{21}}k \quad \bar{G_{22}}k], \quad C_7 \equiv d[(1/2)\bar{G_{21}}e_6 - \rho G_{11}f_6 \quad (1/2)\bar{G_{22}}e_6 - \rho G_{12}f_6]$$

$$\bar{G_{21}} \equiv G_{21} + \rho\delta, \quad \bar{G_{22}} \equiv G_{22} - \rho\delta$$

4.2.2 Dynamic equations

Based on the twist calculated in terms of the independent joint rate vector vector $\dot{\theta}_a$, we now derive the generalized inertia matrix and the matrix of convective inertia term for the coupled equation of motion 4.9.

4.2.2.1 Generalized Inertia Matrix, I

The above equations gives the twist of individual body, i.e $t_i = T_i\dot{\theta}_a$. As defined earlier $t = [t_1^T, t_2^T....t_7^T]^T$ and $t = T\theta$ we get

$$T = [T_1^T, T_2^T, ...T_7]^T$$

Since the matrix M is block diagonal, the inertia matrix of the full system is given by

$$I = T^T M T = T_1^T M_1 T_1 + T_2^T M_2 T_2 + ...T_7^T M_7 T_7 \tag{4.26}$$

We define the contribution of rear wheels alone to the inertia matrix by I_m as

$$I_m = \sum_{i=1,2} T_i^T M_i T_i$$

then

$$I_m = \begin{pmatrix} I_w + (\rho\delta)^2 H + +m_w r^2 & -2(\rho\delta)^2 H \\ -2(\rho\delta)^2 H & I + (\rho\delta)^2 H + +m_w r^2 \end{pmatrix} \tag{4.27}$$

where $M_i \equiv \begin{pmatrix} \tilde{I_w} & 0 \\ 0 & m_w\mathbf{1} \end{pmatrix}$ and $\tilde{I_w} \equiv \begin{pmatrix} I_w & 0 & 0 \\ 0 & H & \\ 0 & 0 & H \end{pmatrix}$. Matrix $\tilde{I_w}$ is the 3×3 moment of inertia matrix of the wheel in co-ordinate frame $\{i, j, k\}$, mass of the motorized wheels is m_w and $mb1$ is the 3×3 identity matrix. If the mass of the platform is

m_p and its moment of inertia about vector k is I_p, then as derived in [23]

$$I_3 = T_3^T M_3 T_3 = I_p(\rho\delta)^2 \begin{pmatrix} 1 & -1 \\ -1 & 1 \end{pmatrix} + m_p r^2 \begin{pmatrix} (1/4)+\gamma^2 & (1/4)-\gamma^2 \\ (1/4)-\gamma^2 & (1/4)+\gamma^2 \end{pmatrix} \tag{4.28}$$

Similarly, if m_c is the mass of the castor wheel and it is assumed to be a solid disk, then the generalized inertia matrix can be written as

$$\begin{aligned} I_c = \sum_{i=4,6} T_i^T M_i T_i = (m_c r^2/4) & \begin{pmatrix} 6F_{11}^2 + \bar{F}_{21}^{\,2} & 6F_{11}F_{12} + \bar{F}_{21}\bar{F}_{22} \\ 6F_{11}F_{12} + \bar{F}_{21}\bar{F}_{22} & 6F_{12}^2\bar{F}_2 2 \end{pmatrix} \\ & + \begin{pmatrix} 6G_{11}^2 + \bar{G}_{21}^{\,2} & 6G_{11}G_{12} + \bar{G}_{21}\bar{G}_{22} \\ 6G_{11}G_{12} + \bar{G}_{21}\bar{G}_{22} & 6G_{12}^2\bar{G}_2 2 \end{pmatrix} \end{aligned} \tag{4.29}$$

If the mass of the brackets, i.e., body #5 and #7, are small compared to the mass of the caster wheels, then the contribution of $T_5^T M_5 T_5$ and $T_7^T M_7 T_7$ can be neglected.

4.2.2.2 Matrix of Convective Inertia term C

The matrix of convective inertia terms of equation 4.9 can be broken down into two parts, $T^T M\dot{T}$ and $T^T WMT$. As given in equations 4.14, 4.15 and 4.16 T_1, T_2, T_3 of the rear wheels and the platform is constant. Therefore $T^T M\dot{T} = 0$. The generalized inertia matrix too is constant for the rear wheels and the platform, so the vector $I_i\omega_i$ is parallel to vector $\omega_i, i = 1..3 \rightarrow \omega \times I\omega = 0 \rightarrow T^T WMT = 0$. This shows that contribution of the rear wheels and the platform to the convective inertia term is zero. Moreover we have considered the mass of the brackets to be zero, so they also do not contribute to the convective inertia term. Hence

$$C = T^T M\dot{T} + T^T WMT = \sum_{i=4,6} T_i^T M_i \dot{T}_i + \sum_{i=4,6} T_i^T W_i M_i T_i \tag{4.30}$$

The expression for the first term is found by using equations 4.19, 4.20, 4.22 and 4.25. The terms $\dot{F}_{ij}$ and $\dot{G}_{ij}$ denote the derivatives of the elements of the matrix F

and G defined in 4.19, 4.20 . To find $\dot{T_4}$ and $\dot{T_6}$ we have used the fact $\dot{e_4} = \omega_4 \times e_4$ and $\dot{e_4} = \omega_6 \times e_6$.

$$T^T M\dot{T} = (m_c r^2/4)\left[\begin{pmatrix} 6F_{11}\dot{F}_{11} + \bar{F}_{21}\dot{F}_{21} & 6F_{11}\dot{F}_{12} + \bar{F}_{21}\dot{F}_{22} \\ 6\dot{F}_{11}F_{12} + \dot{F}_{21}\bar{F}_{22} & 6F_{12}^2\bar{F}_{22} \end{pmatrix} + \begin{pmatrix} 6G_{11}\dot{G}_{11} + \bar{G}_{21}\dot{G}_{21} & 6G_{11}\dot{G}_{12} + \bar{G}_{21}\dot{G}_{22} \\ 6\dot{G}_{11}G_{12} + \dot{G}_{21}\bar{G}_{22} & 6G_{12}^2\bar{G}_{22} \end{pmatrix}\right] \tag{4.31}$$

The second term of equation 4.30 i.e, $\sum_{i=4,6} T_i^T W_i M_i T_i$ evaluates to zero, as shown below. Consider castor wheel (body #4). Using equation 4.22 and W defined in the equation 4.3 we get,

$$T_4^T W_4 M_4 T_4 = [\Theta_4, C_4] \begin{pmatrix} \Omega_4 & 0 \\ 0 & 0 \end{pmatrix} \begin{pmatrix} I_4 & 0 \\ 0 & m_4\mathbf{1} \end{pmatrix} \begin{pmatrix} \Theta_4 \\ C_4 \end{pmatrix} = \Theta_4 \Omega_4 I_4 \Theta_4 \tag{4.32}$$

To evaluate the above equation, we express all the terms in the coordinate system $\{e_4, f_4, k\}$. Moreover, $\omega_4 = \Theta_4 \dot{\theta_a}$, using definition of Θ_4 from equation 4.22 we get $\omega_4 = (F_{11}\dot{\theta}_1 + F_{12}\dot{\theta}_2)e_4 + (F_{21}\dot{\theta}_1 + F_{22}\dot{\theta}_2)k$ and the cros product matrix of ω_4 as

$$\Omega_4 \equiv \begin{pmatrix} 0 & -(\bar{F}_{21}\dot{\theta}_1 + \bar{F}_{22}\dot{\theta}_2) & 0 \\ (\bar{F}_{21}\dot{\theta}_1 + \bar{F}_{22}\dot{\theta}_2) & 0 & -(F_{11}\dot{\theta}_1 + F_{12}\dot{\theta}_2) \\ 0 & (F_{11}\dot{\theta}_1 + F_{12}\dot{\theta}_2) & 0 \end{pmatrix}$$

When the above expressions are substituted in equation 4.32, we get

$$T_4^T W_4 M_4 T_4 = 0, \quad \Rightarrow T^T W M T = 0 \tag{4.33}$$

So the matrix of convective inertia term C of equation 4.9 is evaluated as

$$
\begin{aligned}
C = (m_c r^2/4)\Bigg[& \begin{pmatrix} 6F_{11}\dot{F}_{11} + \bar{F}_{21}\dot{F}_{21} & 6F_{11}\dot{F}_{12} + \bar{F}_{21}\dot{F}_{22} \\ 6\dot{F}_{11}F_{12} + \dot{F}_{21}\bar{F}_{22} & 6F_{12}^2\bar{F}_{22} \end{pmatrix} \\
& + \begin{pmatrix} 6G_{11}\dot{G}_{11} + \bar{G}_{21}\dot{G}_{21} & 6G_{11}\dot{G}_{12} + \bar{G}_{21}\dot{G}_{22} \\ 6\dot{G}_{11}G_{12} + \dot{G}_{21}\bar{G}_{22} & 6G_{12}^2\bar{G}_{22} \end{pmatrix} \Bigg]
\end{aligned}
\tag{4.34}
$$

All the components of equation 4.9 have now been evaluated, except the τ. These are simply the torques exerted by the actuated wheels. This completes the dynamic model of the WMR with generalized caster wheel configuration.

4.3 Special cases

4.3.1 Standard caster ($d_1 = 0$)

The standard caster wheel configuration can be obtained by setting the value of $d_1 = 0$. In such condition, the left hand side matrix of equations 4.19 and 4.20 become a diagonal matrix. Therefore, the first and second equation of 4.19 and 4.20 get divided by d_2 and r, respectively. The resulting equations relating the unactuated joint rate to actuated joint rates are similar to those reported by [22],[23].

4.3.2 Under Actuated Case ($d_2 = 0$)

It can be seen from equation 4.19 that when the *caster offset* $d_2 = 0$, the LHS matrix becomes singular. So the unactuated joint rates cannot be determined from $\dot{\theta}_a$. It is therefore essential to have proper caster offset in case we need caster like behaviour from a passive wheel.

Another solution is to put an extra actuator to control the bracket motion by controlling ψ_i. As in the case of Ackerman steering mechanism, where the steering wheel controls the orientation of the front passive wheels of a car.

4.4 Simulation

The mobile manipulator proposed in chapter 3 was modelled as a differential drive robot. The front wheels and steering mechanism were not included in the dynamic model as their masses are too small compared to the platform. The weight of each wheel is 0.3Kg, the steering mechanism 0.24Kg, whereas the weight of the platform is 70Kg.

In simulation the vehicle, (point O_3), is required to trace a circle of radius 5m. As shown in the figure 4.4. β is the angle between the line joining point O_3 and the origin O with respect to $X-axis$. The function $\beta(t)$ is defined such that the ful circle is completed in 60Sec.

$$\beta(t) = \frac{20\pi}{60^3}t^3 - \frac{30\pi}{60^4}t^4 + \frac{12\pi}{60^5}t^5 \tag{4.35}$$

Moreover the velocity and acceleration of the robot is zero at the beginning (t=0) and end of travel (t=60). The initial pose of the vehicle is parallel to the $Y-axis$ i.e. $\beta = 0$ shown by dotted line in figure 4.4.

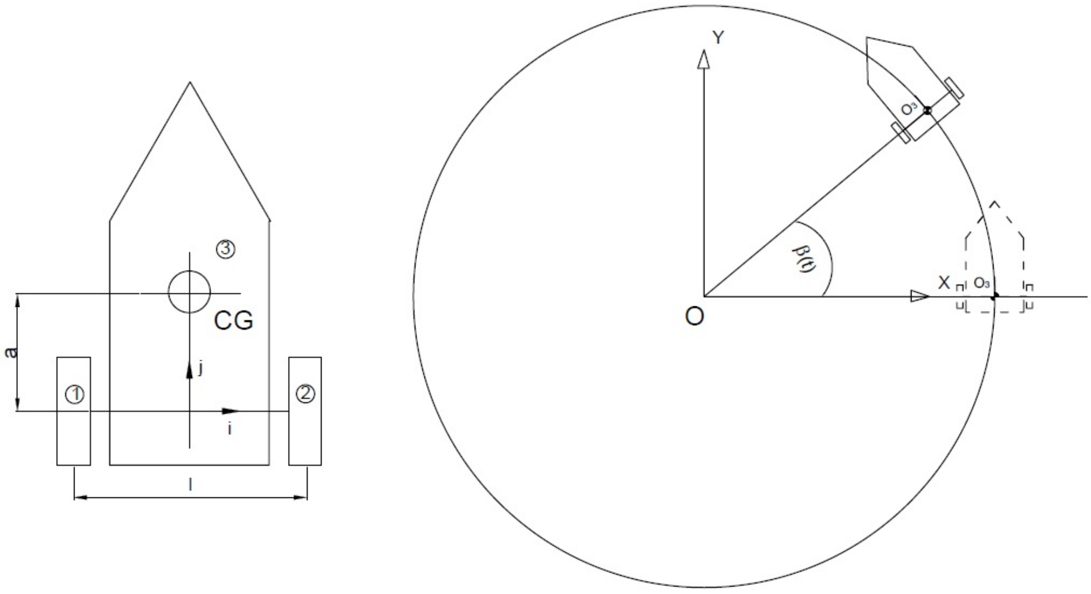

Figure 4.4: Path Traced by Robot

4.4.1 Inverse Dynamics

Using the model inverse kinematic, the wheel velocity and acceleration are determined using pseudo Inverse The wheel angle, velocity and acceleration were used in the dynamics equation to calculate the torque required by each motor. The results are plotted in figure 4.5.

The equation of dynamic model is given in equation 4.36, where the actuated joints are $\theta_a(t) = (\theta_l, \theta_r)$ are the rear left and right wheel rotation angles. The dynamic and kinematic parameters used in the simulation is listed in table 4.1. The rear wheels ($i = 1, 2$) and the platform $i = 3$, twist $t_i^T = T_i\theta_a$, is given in equations 4.14,4.15 and 4.16. The dynamic equation is of the vehicle on slope is given as

$$\begin{aligned} T^T M T\ddot{\theta}_a &= -T^T(M\dot{T} + WMT)\dot{\theta}_a + T^T(w^J + w^G) \\ \text{where} \quad T &= (T_1^T T_2^T T_3^T)^T, \quad M = diag(M_1, M_2, M_3) \\ T^T M T &= I_1 + I_2 + I_m + I_3 = I_m + I_3 \\ W &= diag(W_1, W_2, W_3), \quad w^G = g\sin\alpha, \quad \alpha = 10^o \end{aligned} \tag{4.36}$$

w^G, w^J and α represent the gravitational force acting along the inclined the external torque/Force applied by a motor and the inclination of the plane to horizontal respectively. The generalized inertia matrix I_m and I_3 are given in 4.27 and 4.28. As stated earlier the convective inertia term is zeros a the inertia matrices are constant. The motor torque are then given a

$$T1^T w_1^j = \tau_1, \quad T_2^T w_2^j = \tau_2 \tag{4.37}$$

$$T_3^T w^g = \begin{pmatrix} \rho\delta k & r(\lambda i + (1/2)j) \\ -\rho\delta k & r(-\lambda i + (1/2)j) \end{pmatrix} \begin{pmatrix} 0 \\ -jg\sin\alpha \end{pmatrix} = \begin{pmatrix} -\frac{1}{2}rg\sin\alpha \\ -\frac{1}{2}rg\sin\alpha \end{pmatrix} \tag{4.38}$$

The torques required at the wheels of the vehicle to move up a spiral ramp of slope 10^o and radius 5m is given figure 4.5.

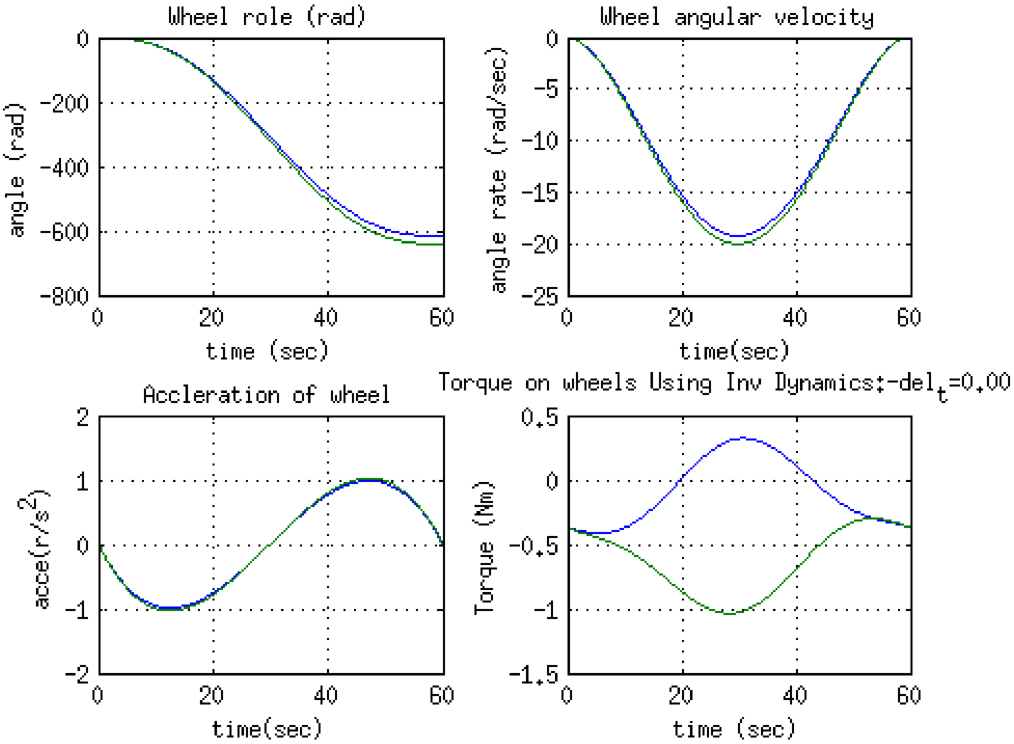

Figure 4.5: Inverse dynamics of the mobile robot

Table 4.1: Dynamic & kinematic parameters

Part Name	*Property*	*Value*
Rear Wheels	mass	300g
	Moment of Inertia	diag(242, 242, 465)kg mm^2
Base Frame	mass	70Kg
	Moment Of Inertia	$\begin{pmatrix} 1.18 & 0.01 & -0.05 \\ 0.01 & 1.28 & 0.08 \\ -0.05 & 0.08 & 0.53 \end{pmatrix} Kg - m^2$
l	length	400mm
r	wheel radius	100mm
a	see figure	

4.5 Summary

In this chapter the dynamic equation was derived for the most general form of caster wheel configuration. Even though only two caster wheel configuration was considered the same formulation can be extended to any number of caster wheels. It is shown that the dynamics of standard caster wheels is a special case of the general case with $d_1 = 0$.It is also proven why a caster needs non-zero caster offset. There is a need of extra actuator in case $d_2 = 0$.

Chapter 5

Control of mobile manipulator

In this chapter the control architecture of the teleoperated mobile robot is presented. The user interface for teleoperation is discussed. The control algorithm running on the mobile robot and the hardware used for the control of traction and steering is discussed. The protocol used for communication between the robot and user interface also described in detail.

5.1 Control Architecture and Hardware

The mobile manipulator is planned to be teleoperated over a wireless network. The control block diagram and architecture are shown in Figure 5.1. It has a remote control station which is the interface for the operator and a local controller

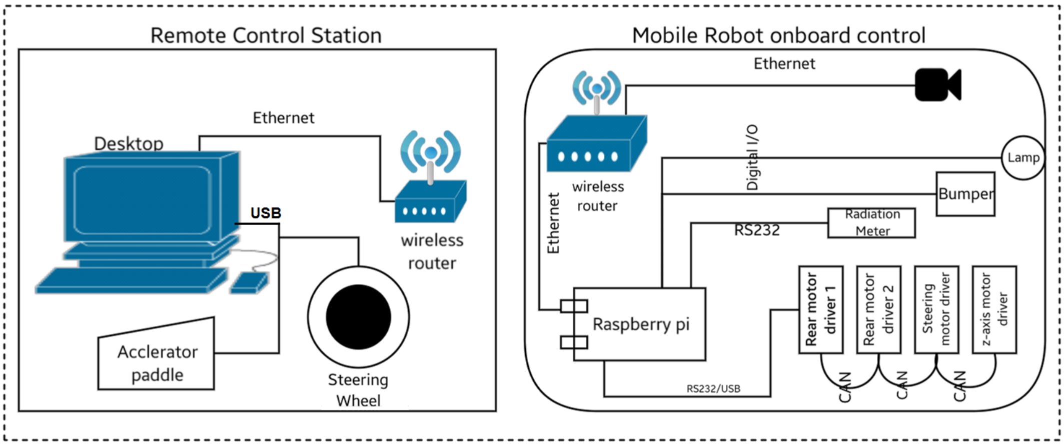
Remote Control Station
Desktop
Ethernet
USB
wireless router
Acclerator paddle
Steering Wheel
Mobile Robot onboard control
Ethernet
wireless router
Ethernet
Digital I/O
Lamp
Bumper
Radiation Meter
RS232
Raspberry pi
RS232/USB
Rear motor driver 1
Rear motor driver 2
Steering motor driver
z-axis motor driver
CAN
CAN
CAN

Figure 5.1: Control Architecture Block Diagram

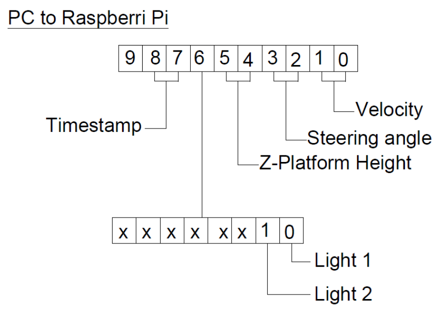

Figure 5.2: Data sent from PC to Onboard controller

on the mobile manipulator. They communicate over dedicated wireless network. The remote station send data packet every 50 millisecond (20Hz) to the mobile manipulator. The commanded velocity, the steer angle, the z position of the platform and the state of the detector and headlamps constitutes the data packet sent by the remote station as shown in 5.2. The on board control of the mobile robot replies with a data packet consisting of the X, Y position and orientation θ of the robot, the current steer angle, angular velocities of each wheels, the z position of the top platform, battery voltage and current of each motor.

5.1.1 Local Onboard Controller

The on-board computer which is Raspberry Pi running raspian (linux) os receives the command from the remote station and controls the robot hardware through customized c++ application. The raspberry pi is daisy chained to the four Maxon EPOS2 motor controllers/drivers. The communication between the onboard computer and the first Maxon controllers is over usb/RS232 interface using Maxon's proprietorial protocol [25]. The first controller serves as CAN master for the rest of the controllers. The rear wheel motor drivers are configured in velocity servo loop. The steering and the z-axis motors drivers are configured in position control loop. The camera mounted on the mobile robot and Raspberry Pi is connected over Ethernet via a wireless hub. the wiring digram of the robot is given figure 5.3. Since the onboard camera is connected to the wireless net work directly, therefore it does not interfere with the command loop between the raspberri Pi and the PC.

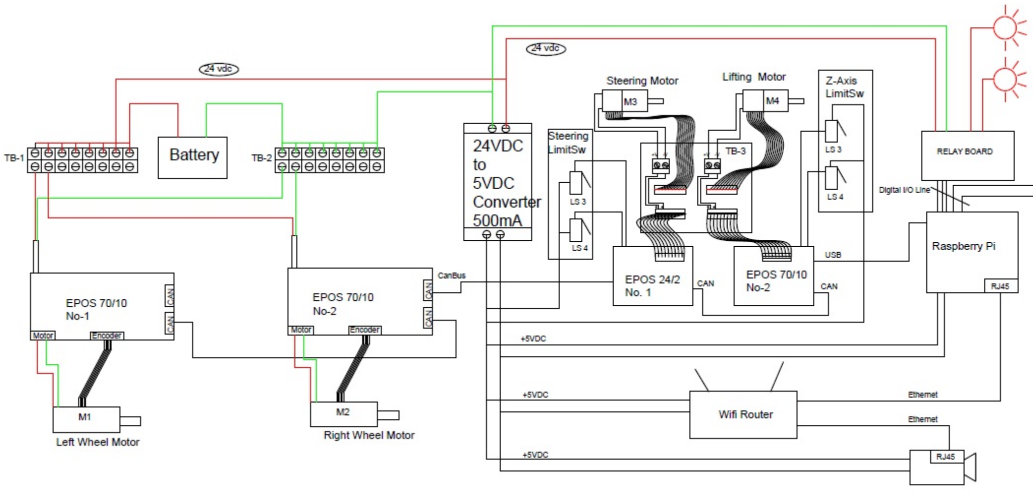
24 vdc
24 vdc
TB-1
Battery
TB-2
24VDC to 5VDC Converter 500mA
Steering Motor
M3
Lifting Motor
M4
Z-Axis LimitSw
Steering LimitSw
LS 3
LS 4
TB-3
LS 3
LS 4
RELAY BOARD
Digital I/O Line
LS 1
LS 2
Bumper LimitSw
Raspberry Pi
RJ45
USB
EPOS 24/2 No. 1
CAN
EPOS 70/10 No-2
CAN
CanBus
EPOS 70/10 No-1
CAN
CAN
Motor
Encoder
EPOS 70/10 No-2
CAN
CAN
Motor
Encoder
M1
Left Wheel Motor
M2
Right Wheel Motor
+5VDC
+5VDC
Wifi Router
Ethernet
Ethernet
+5VDC
RJ45

Figure 5.3: Wiring Diagram of Robot

The mobile robot is teleoperated using position-speed command as in [26] is used as the work space for the mobile robot is infinite compared to input device. In case of manipulators position-position control approach is used with scaling. In our case we user the mixed approach. The steering angle is controlled in position -position mode where as the mobile robots speed is controlled by foot paddle's position, i.e. position-velocity mode. This is given by the following equation

$$\begin{pmatrix} V \\ \theta_S \end{pmatrix} = \begin{pmatrix} K_v & 0 \\ 0 & K_s \end{pmatrix} \begin{pmatrix} \tilde{X_p} \\ \tilde{\Theta}_s \end{pmatrix} \tag{5.1}$$

where $\tilde{X_p}$ is the displacement of paddle, $\tilde{\theta_s}$ is the twist in steering wheel, K_v and K_s are the proportionality constants, V is the velocity of point O_3 and θ_s is the displacement of the steer motor. These proportionality constants are derived as below bases on extreme limits.

Table 5.1: Proportionality constant table

Robot parameters	range	Joy-Stick Parameter	range	parameter Value
θ_s	-60 to +60	$\tilde{\Theta}_s$	-90^o to 90^o	$K_s = 2/3$
V	0 to +60 mm/sec	$\tilde{X_p}$	0 to 30mm	$K_v = 2$

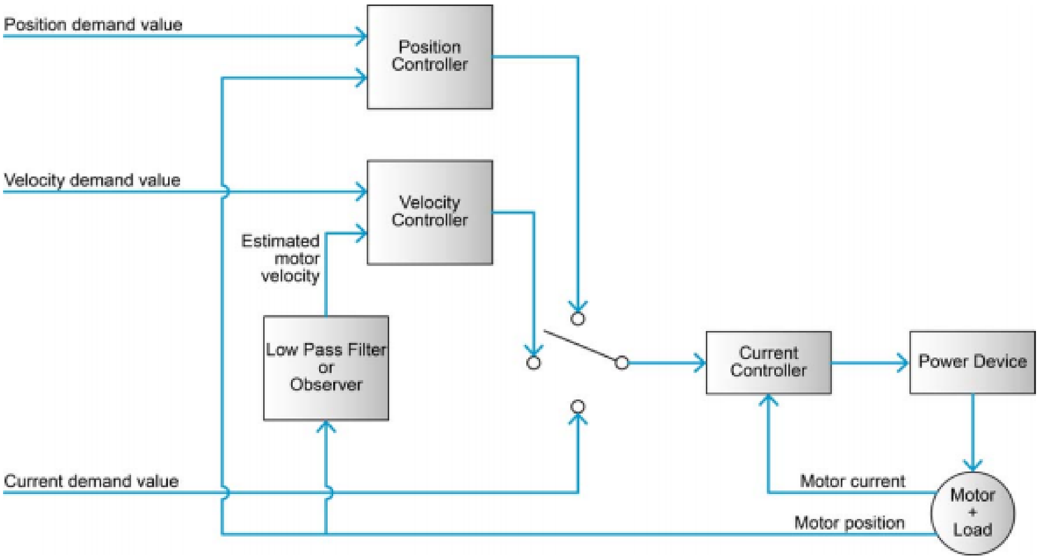
Position demand value
Position Controller
Velocity demand value
Velocity Controller
Estimated motor velocity
Low Pass Filter or Observer
Current Controller
Power Device
Current demand value
Motor current
Motor position
Motor + Load

Figure 5.4: EPOS4 Controller Block Digram

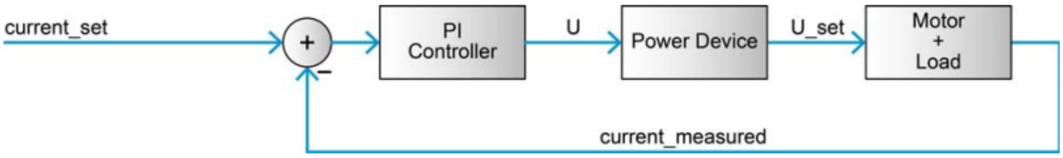
current_set
+
−
PI Controller
U
Power Device
U_set
Motor + Load
current_measured

Figure 5.5: Current control bolck digram

5.1.2 Details of Motor Controller

Three EPOS2 controller from Maxon Motors is used to control the mobile robots rear wheel velocity and the steering gear position. Each controller can control one motor. The over architecture of the controller as given in [27], [28] and is shown here in figure 5.4. The controller can be configured in either current, position or velocity control mode. The inner most current loop controls the torque of the motor. The current feedback loop shown in figure 5.5 is a PI loop running at 25KHz and the transfer function of the PI block is given in equation 5.2.

$$C(s) = K_p + \frac{K_I}{s} \tag{5.2}$$

where K_p and K_I are the proportional and Integral gains.

The rear motor controllers are configured to in velocity mode. The block digram of the velocity loop is given in figure 5.6. The velocity controller is a PI controller with velocity and acceleration feed-forward. The transfer function $V(s)$of velocity loop PI block is given by

$$V(s) = K_{p\omega} + \frac{K_{I\omega}}{s} \tag{5.3}$$

where $K_{p\omega}$ and $K_{I\omega}$ are velocity proportional and integral gain respectively. The sampling rate of the velocity loop is 2.5 KHz. The feedforward accleration and feedforward velocity is used to compensate for the known inertial load and viscous frictional load [28]. The lowpass filter used in 5.4 is used because velocity is estimated from differentiating the position, the filter eliminates noise due to differentiation. The transfer function $H(s)$ of lowpass filter is given below

$$H(s) = \frac{1}{1 + \frac{K_{p\omega}}{48K_{I\omega}}} \tag{5.4}$$

The gain values used for each rear motor in the velocity control mode is listed in table 5.3 and 5.2. No acceleration or velocity feedforward was used. These parameters were determined by auto tuning.

Table 5.2: Rear Right Motor Controller parameters

Gain Parameter	*Value*	*Unit*
K_p	300	$\frac{mV}{A}$
K_I	100	$\frac{mV}{A.mS}$
$K_{P\omega}$	1000	$\frac{mA.sec}{rad}$
$K_{I\omega}$	100	$\frac{mA}{rad}$

Table 5.3: Rear Right Motor Controller parameters

Gain Parameter	*Value*	*Unit*
K_p	230	$\frac{mV}{A}$
K_I	53	$\frac{mV}{A.mS}$
$K_{P\omega}$	5182	$\frac{mA.sec}{rad}$
$K_{I\omega}$	425	$\frac{mA}{rad}$

The steering motor is in position control mode. The block digram is shown in

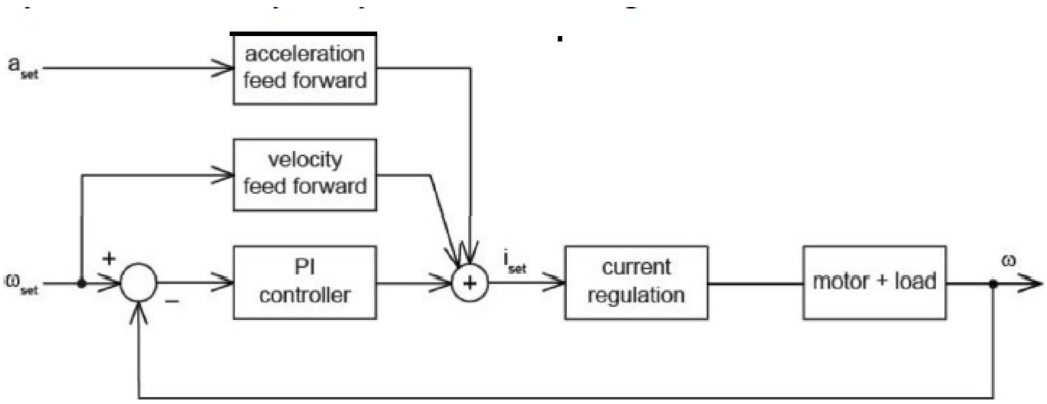
a_{set}
acceleration feed forward
velocity feed forward
+
ω_{set}
–
PI controller
+
i_{set}
current regulation
motor + load
ω

Figure 5.6: Velocity control bolck digram

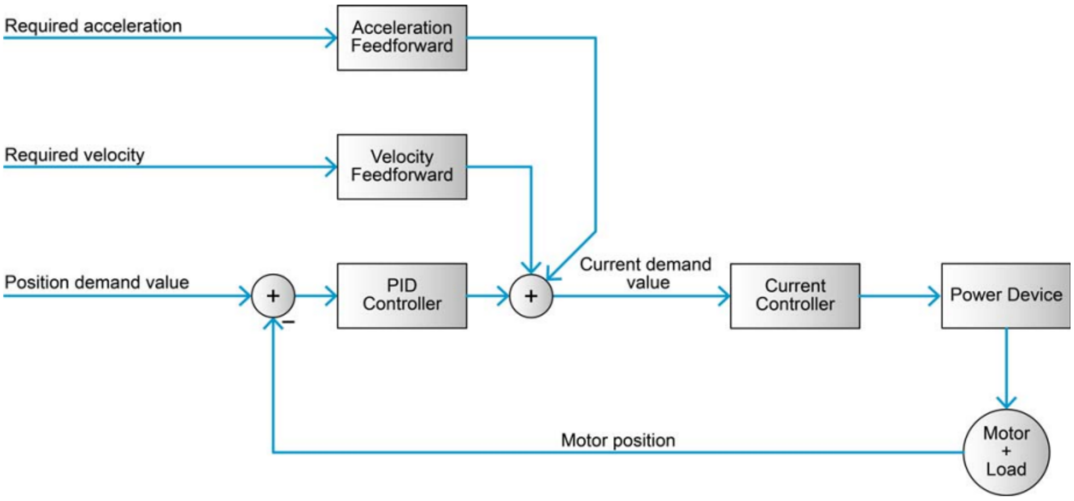
Required acceleration
Acceleration Feedforward
Required velocity
Velocity Feedforward
Position demand value
+
–
PID Controller
+
Current demand value
Current Controller
Power Device
Motor + Load
Motor position

Figure 5.7: Position control bolck digram

figure 5.7. It is a PID controller with transfer function given as

$$P(s) = K_{PP} + K_{IP}s + \frac{K_{DP}s}{1 + \frac{K_{DP}}{10K_{PP}}s} \tag{5.5}$$

where K_{PP}, K_{IP} and K_{DP} are position proportional, integral and derivative gains. The velocity $F_{\omega P}$ and acceleration $F_{\alpha P}$ are also used in position control loop to take care of viscious friction and known inertial load. The gains for controller was decided using auto tuning software provided by Maxon Motors. The value are reported in table 5.4.

Table 5.4: Rear Steer Motor Controller parameters

Gain Parameter	*Value*	*Unit*
K_p	537	$\frac{mV}{A}$
K_I	307	$\frac{mV}{A.mS}$
K_{PP}	128	$\frac{mA.sec}{rad}$
K_{IP}	663	$\frac{mA}{rad}$
K_{ID}	200	$\frac{mA}{rad}$
$F_{\omega P}$	0	$\frac{mA.sec}{rad}$
$F_{\alpha P}$	54	$\frac{mA.sec^2}{rad}$

5.1.3 The control algorithm for platform

Thsi section discusses the in detail the algorithem running of the on-board controller. Command received by the controller is parsed to extract the velocity and the steer angle information and suitably scaled to get command velocity V, in mm/sec and steering angle θ_s in radians. It may be noted that the velocity v corresponds to the velocity of point O_r the reference point of the mobile robot. Next based the set point for each motor is calculated and sent to individual drives. The algorithm is listed below and the block digram for the same in figure 5.8

1. Calculate the setpoint for steering motor θ_{SM} based on θ_s
2. Read the current steering angle ϕ_{ic}.
3. Calculate the rear wheel velocities setpoints ω_i and ω_o based on the V and ϕ_{ic}

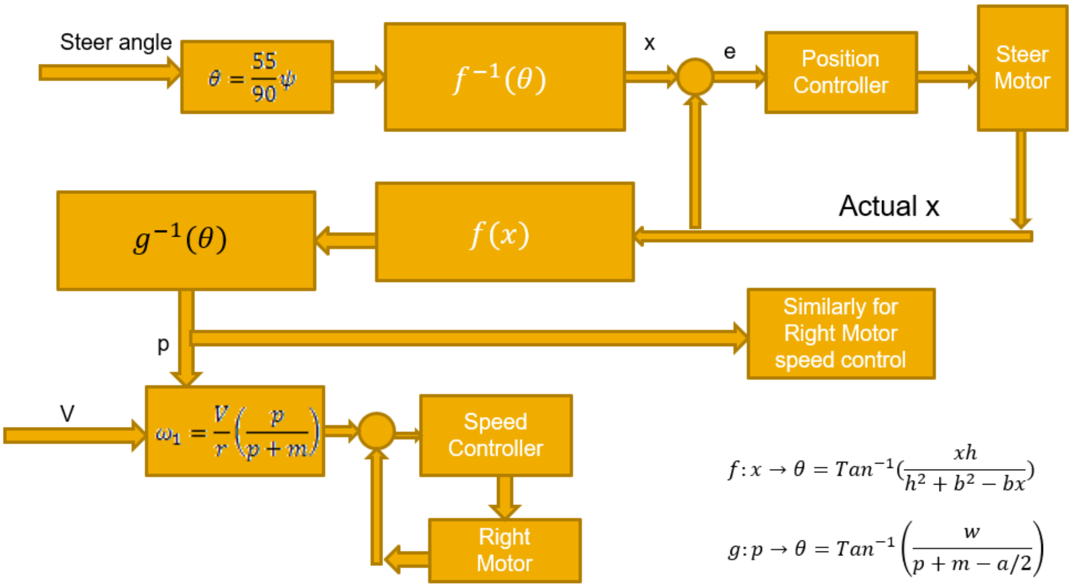
Steer angle
$\theta = \frac{55}{90}\psi$
$f^{-1}(\theta)$
x
e
Position Controller
Steer Motor
Actual x
$g^{-1}(\theta)$
$f(x)$
p
Similarly for Right Motor speed control
V
$\omega_1 = \frac{V}{r}\left(\frac{p}{p+m}\right)$
Speed Controller
Right Motor
$f: x \rightarrow \theta = Tan^{-1}(\frac{xh}{h^2+b^2-bx})$
$g: p \rightarrow \theta = Tan^{-1}\left(\frac{w}{p+m-a/2}\right)$

Figure 5.8: provide suitable title

4. command set points ω_i, ω_o and θ_{SM} to each motor

The above loop is repeated every 50 mSec.

It may be noted that the steer angle command received from the control station is not directly sent to the steer motor as set point after suitable scaling. The steer set point is based on the current rear wheel velocities. This important as the response time of the motors are different. The above methodology helps minimize deviation from the Ackerman steering condition even during transit condition, particularly in case of large change in commanded v and θ_s. Each block in the figure 5.8 is discussed next.

It may be noted that the θ_s always refers to the steer angle of the inner front wheel ϕ_i and V refers to O_r as shown in figure **??**, i.e.

$$\theta_s = \phi_i \tag{5.6}$$

The set point of the steering motor at the output of gear box θ_{SM} is given by equations 5.7 and 5.8 based on the geometry of Davis steering gear [10].

$$\tan\phi_i = \frac{xh}{h^2 + b^2 - bx}$$

or

$$f : \phi_i \to x, \quad x = \frac{\tan\phi_i(h^2 + b^2)}{h + b\tan\phi_i} \tag{5.7}$$

where x is the displacemet of the rack and h and b are link lengths. The rack is connected to the steering motor by pinion of pcd (D_p) 30mm as shown in the figure **??**. Therefore the set point for the steering motor is given below as

$$\theta_{SM} = x\frac{360}{\pi D_p} \tag{5.8}$$

Next we present the equation relating current steer angle ϕ_{ic} and rear wheel set point velocities ω_{RS} and ω_{LS}. From the geometry of figure **??** we get

$$\begin{aligned} \tan\phi_{ic} &= \frac{\bar{BD}}{\bar{OB}} = \frac{w}{p + m - a/2} \\ g : \phi_{ic} \to p, \qquad p &= \frac{w}{\tan\phi_{ic}} - m + \frac{a}{2} \end{aligned} \tag{5.9}$$

Now using 4.10 and 4.11 in equations

$$\dot{O}_r = \dot{O}_i + \omega_3 \times (O_r - O_i)$$
$$\dot{O}_r = \dot{O}_o + \omega_3 \times (O_r - O_o)$$

the rear wheel velocities are calculated as

$$\omega_i = \frac{Vp}{r(p + m)}$$
$$\omega_o = \frac{V(p + 2m)}{r(p + m)}$$

using the above equation and 5.9. We get the setpoints for the rear wheels

$$\omega_i = \frac{V}{r} \frac{(\frac{w}{\tan\theta_o} - m + \frac{a}{2})}{\frac{w}{\tan\theta_o} - m + \frac{a}{2} + m} \tag{5.10}$$

$$\omega_o = \frac{V}{r} \frac{(\frac{w}{\tan\theta_o} - m + \frac{a}{2}) + 2m}{\frac{w}{\tan\theta_o} - m + \frac{a}{2} + m} \tag{5.11}$$

- calibration of steer data and wheel velocity

5.1.3.1 Wheel odometry

The dead reconning odometery can be performed based on the differential drive model ot the bicycle model. In the present case we use the differential drive model, i.e the rear wheel velocities are used to determine the position and orientation of the mobile robot. The position here means the position of reference point O_3. The steps are follower

1. calculate V and ω_3 from current wheel velocities ω_1 and ω_2 using equations 4.11 and 4.12 with $a = 0$.
2. integrate V and ω_3 over time step.

If $x(t)$, $y(t)$ is the location of O_r and $\beta(t)$ the orientation of robot with some global coordinate system the kinamitic model of the differential wheel robots as given in [15] is

$$\begin{pmatrix} \dot{x} \\ \dot{y} \\ \dot{\beta} \end{pmatrix} = \begin{pmatrix} \cos\beta & 0 \\ \sin\beta & 0 \\ 0 & 1 \end{pmatrix} \begin{pmatrix} V \\ \omega_3 \end{pmatrix} \tag{5.12}$$

which is numerically integrated for time δt using the equations

$$x(i+1) = x(i) + \delta t * \cos(\beta(i)) * V(i); \tag{5.13}$$

$$y(i+1) = y(i) + \delta t * \sin(\beta(i)) * V(i); \tag{5.14}$$

$$\beta(i+1) = \beta(i) + \delta t * \omega_3(i); \tag{5.15}$$

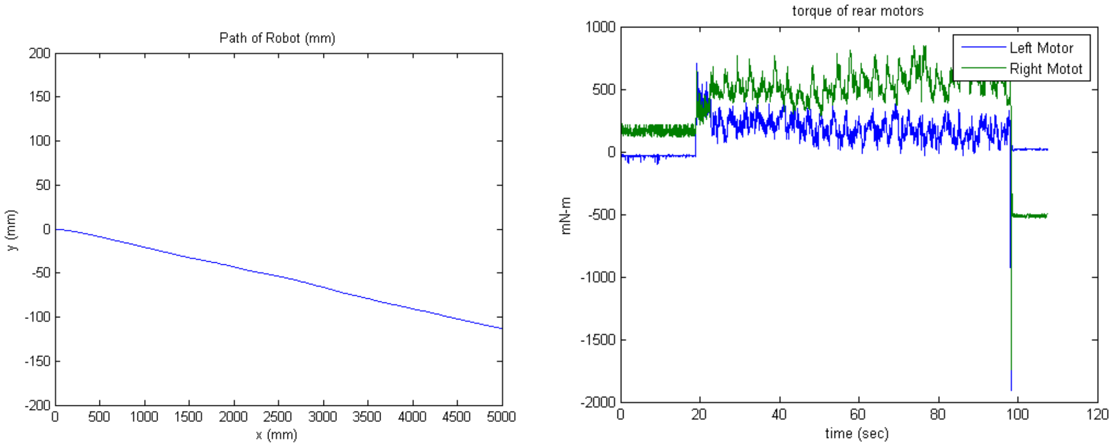

Figure 5.9: Tracing a line

Figure 5.10: Motor torque

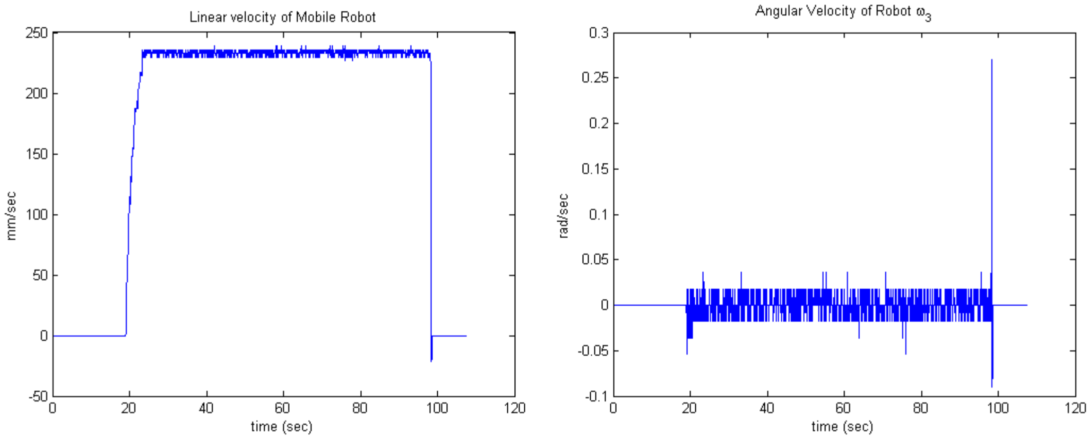

Figure 5.11: Linear Velocity

Figure 5.12: Angular Velocity

Figure 5.13: Linear motion of WMR

where i is at time step t_i. Next we present the actual odometric results for the vehicle moving in a circle and a straight line.

5.1.3.2 Control of Z platform

Decentralized control technique treats the manipulator and the platform as two different system. The inter-coupling forces are treated as external forces on the system. The dynamics equation of the mobile manipulator can thus be split as follows [3].

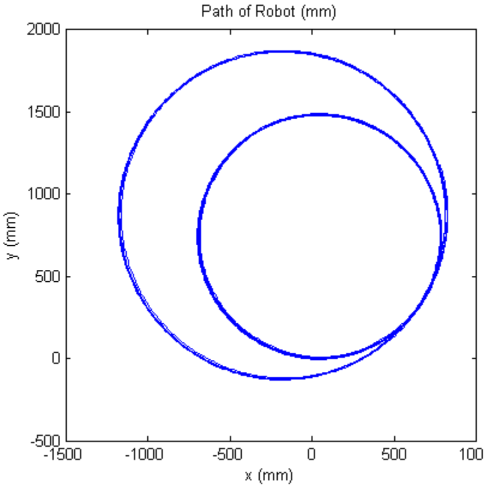

Figure 5.14: Tracing a Circle

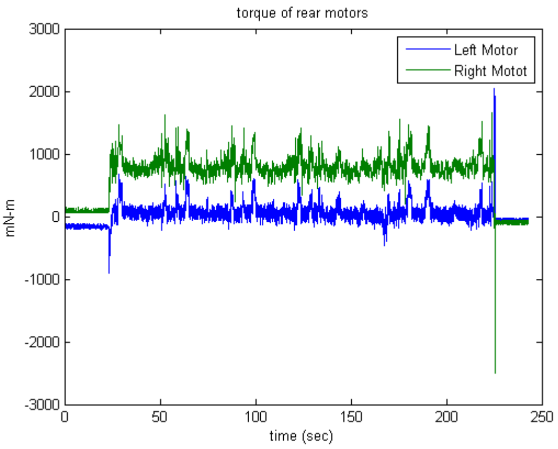

Figure 5.15: Motor torque

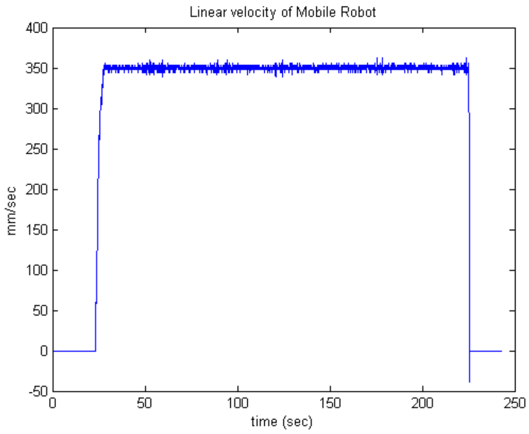

Figure 5.16: Linear Velocity

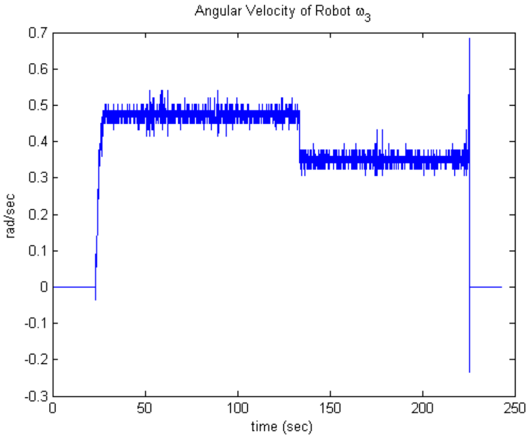

Figure 5.17: Angular Velocity

Figure 5.18: Circular motion of WMR

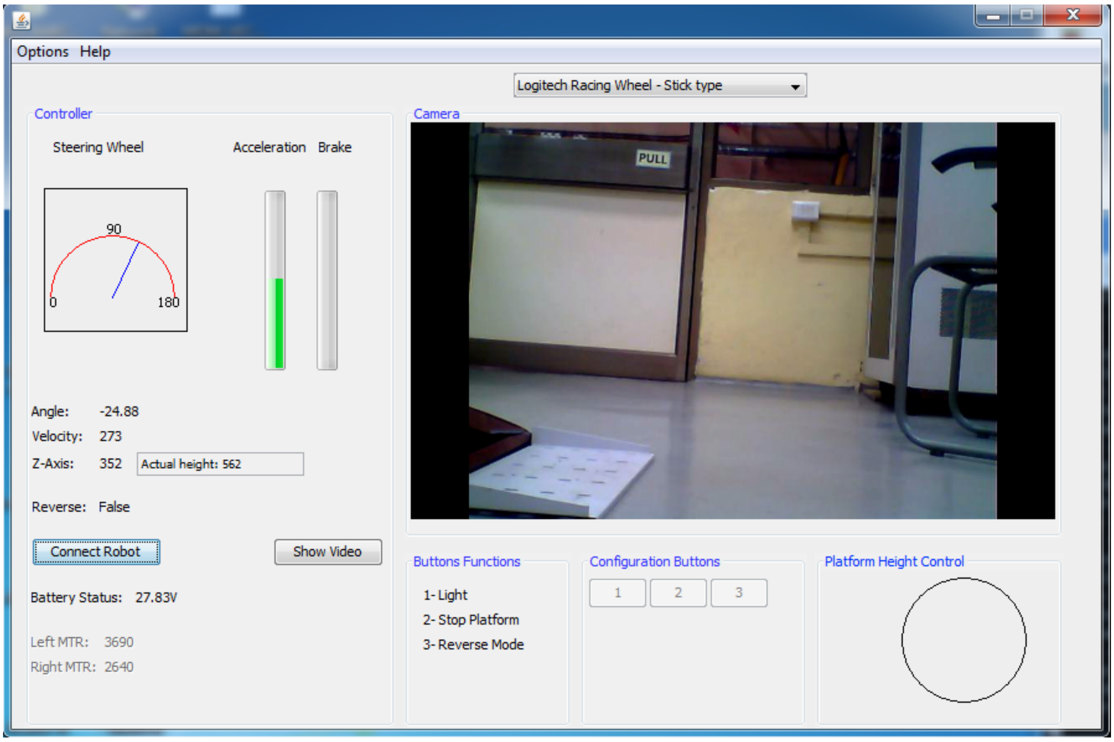
Options Help
Controller
Steering Wheel
Acceleration
Brake
90
0
180
Connect Robot
Show Video
Camera
PULL
Buttons Functions
Configuration Buttons
1
2
3
Platform Height Control

Logitech Racing Wheel - Stick type

Angle: -24.88
Velocity: 273
Z-Axis: 352 Actual height: 562
Reverse: False
Battery Status: 27.83V
Left MTR: 3690
Right MTR: 2640

1- Light
2- Stop Platform
3- Reverse Mode

Figure 5.19: User Interface for teleoperation

5.1.4 The Remote Control Station

The local station consists of a desktop computer running Windows XP. A Steering wheel and two foot switches are connected to the desktop. The steering wheel is used for turning mobile robot. One of the two foot switch acts as an accelerator to set the mean velocity the other is used to brake the vehicle.

The screen of the desktop displays the video streaming from the mobile robot on board camera. A graphical user interface (GUI) also displays the robot's parameters such as current steer angle, velocity of each rear wheel and the position of the z-axis. Buttons on the GUI operates the z-axis, head lamps, etc.

5.2 Summary

In this chapter,

Chapter 6

Simulation Time Delay Tele-operation

In this chapter simulation of a teleoperated mobile platform is presented. In teleoperation the human operators observe a remote scene through camera/s, and manipulating the local steering wheel and accelerator paddle as shown in figure 6.1 . The command is transmitted to the mobile robot over wireless network. The operator response is based on the latest feedback images from the cameras. In general there is time lag when communication take place over wireless network. The time lag deteriorates the human performance as discussed in [29] and references there in. The this chapter simulation of teleoperation both for delayless and delay transmission network are presented.

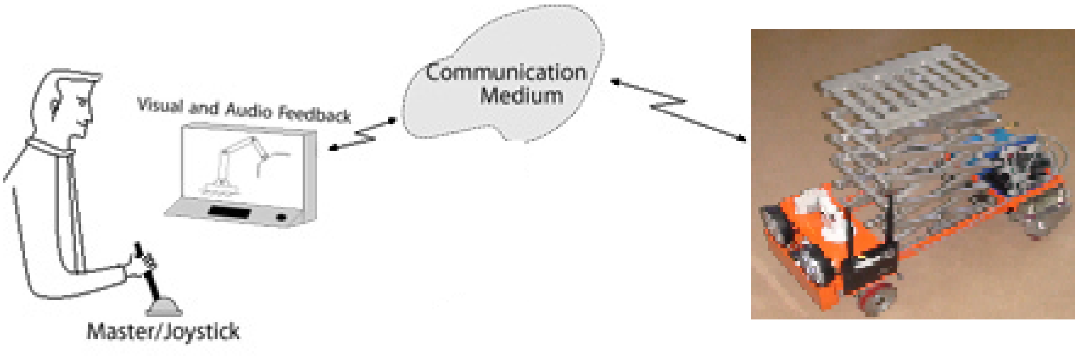

Figure 6.1: Teleoperation Architecture

6.1 Modeling of mobile platform

The standard kinematic model as described in [15] of the mobile platform is used for the simulation. This use of kinematic is justified as the vehicle is expected to move at relatively slow speed and model is simple. Inputs to the model are left and right rear wheel velocities. The front wheels are steered to satisfy the Ackerman condition as presented in **** and are assumed to attain the desired angle instantaneously. Therefore the robot can be treated as differential drive robot. The kinematic model of the platform is presented below

$$\begin{pmatrix} \dot{x} \\ \dot{y} \\ \dot{\theta} \end{pmatrix} = \begin{pmatrix} \cos\theta & 0 \\ \sin\theta & 0 \\ 0 & 1 \end{pmatrix} \begin{pmatrix} r_w/2 & r_w/2 \\ 1/b & -1/b \end{pmatrix} \begin{pmatrix} \dot{\phi_L} \\ \dot{\phi_R} \end{pmatrix} \tag{6.1}$$

Where , b is the distance between the rear wheels, r_w wheel radius. $\dot{\phi_R}$ and $\dot{\phi_L}$ are the left and right wheel rotational velocity.

The operator station sends the command u_1 and u_2 over the wireless network, in general it will be delayed by δ time. These commands are interpreted by the robot controller as the left and right wheel velocities. Therefore by taking the time delay into consideration we can write

$$\begin{pmatrix} \dot{\phi_R}(t) \\ \dot{\phi_L}(t) \end{pmatrix} = \begin{pmatrix} u_r(t-\delta) \\ u_1(t-\delta) \end{pmatrix} \tag{6.2}$$

The control inputs to the mobile robot u_1 and u_2 are generate by the operator based on the visual data available to him. We next present the model of the human operator to be used for simulation the complete loop.

6.2 Modeling the human operator

In order to simulate the teleoperation loop we need a mathematical model of human operator. The mathematical modelling of the operator‘s action is modelled

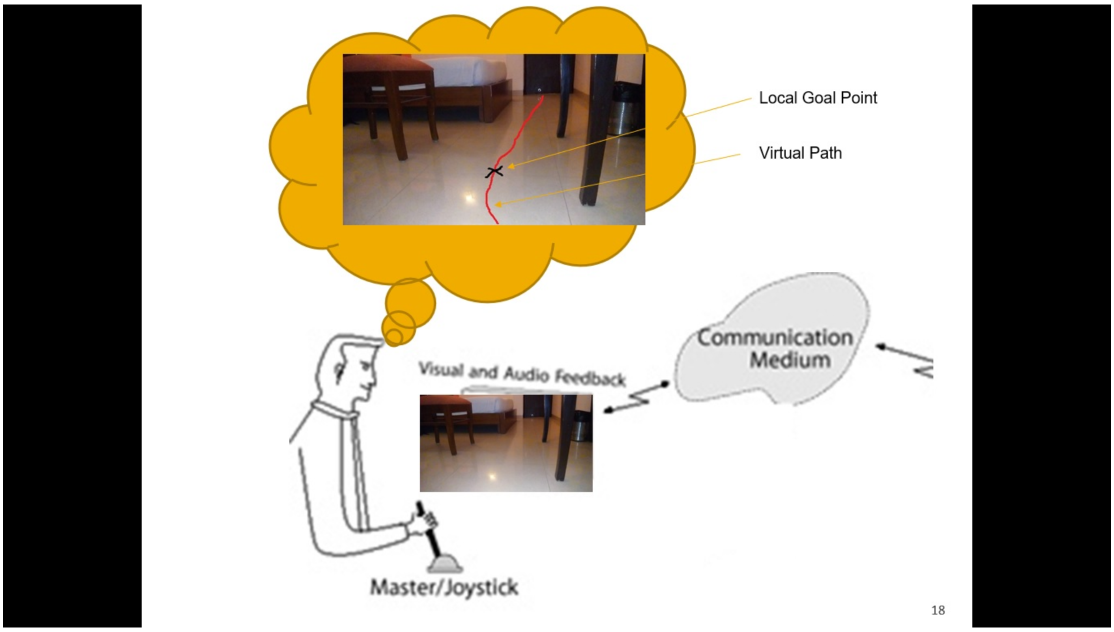

Figure 6.2: Assumed driving strategy

assuming a car driving metaphor. The video feedback, which the he receives of the remote environment, give him the idea of the vehicles position and the tentative next goal point (p) based on a lookahead distance (l). He then constructs a virtual path mentally and tries to manoeuvre or steers the robot to follow that path as shown in figure 6.2. As he moves forward the goal point keeps changing until he reaches the desired location. This methodology of path tracing is known as pure pursuit [30] or following the carrot strategy.

The mathematical model for the pure pursuit method of path following can be derived as given in figure 6.3. As shown in figure 6.3, the origin of the coordinate system is at point o, the middle of rear axis of the robot. Since the differential drive robot can move only about a circle with center lying on the line along its rear axis, a arc op of radius r, is drawn with center $o1$ and passing through o and p. Where p is a point on the path to be traced by the robot. The linear distance l between the points o and p is called the look ahead distance. This distance in the case of a teleoperated robot will depend on the field of view of the remote location camera and the obstacles in present in the remote environment.

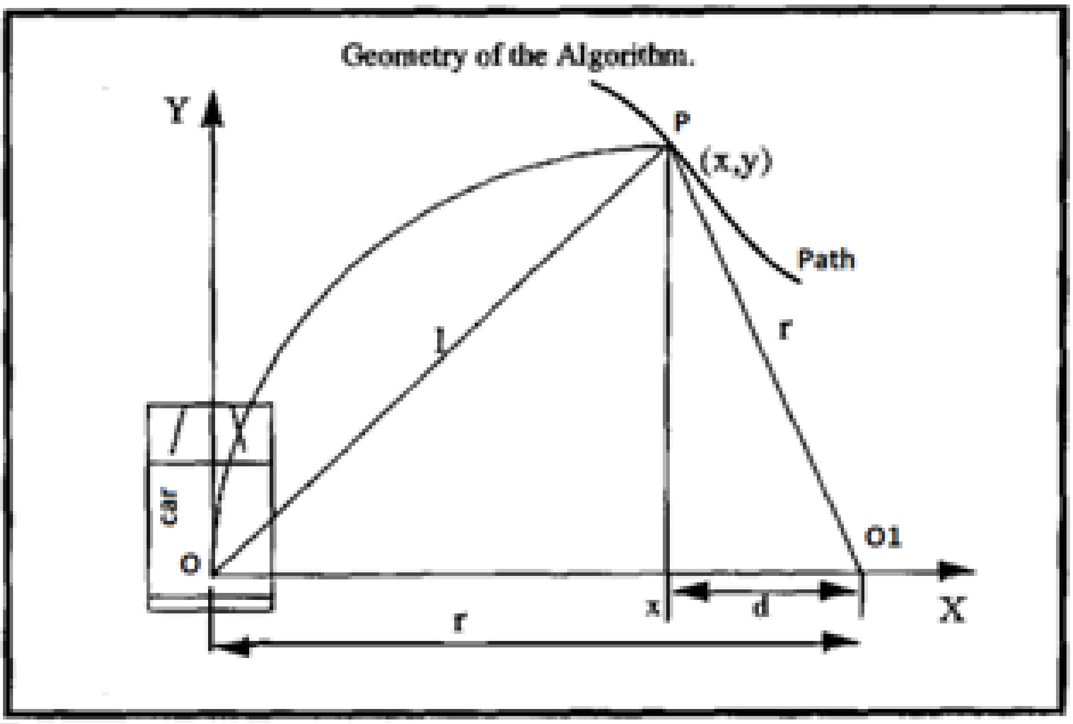

Figure 6.3: Geometry of Pure Pursuit

If (x, y) is the coordinate of point p in $X - Y$ coordinate system, then

$$x^2 + y^2 = l^2, \qquad d = r - x \tag{6.3}$$

Similarly, from triangle $p, x, o1$ we get

$$d^2 + y^2 = r^2 \quad \Rightarrow (r - x)^2 + y^2 = r^2 \quad \Rightarrow x^2 + y^2 - 2rx = 0 \tag{6.4}$$

Replacing x^2 and y^2 in equation 6.4 with 6.3 we get

$$2rx = l^2 \qquad \Rightarrow r = \frac{l^2}{2x} \tag{6.5}$$

Once, the radius r the desired linear velocity v of robot is known the angular velocity of the vehicle is $\dot{\theta} = -v/r$. The rear wheel desired velocities $\dot{\phi_d(t)}$ and $\dot{\phi_(t)}$ can be calculated from equation 6.1. Where $\dot{y} = v$ and to match the orientation of vehicle with that in figure 6.3 we set $\theta = 90^o$. We get

$$\begin{pmatrix} \dot{x} \\ \dot{y} \\ \dot{\theta} \end{pmatrix} = \begin{pmatrix} 0 & 0 \\ r_w/2 & r_w/2 \\ b/2 & -b/2 \end{pmatrix} \begin{pmatrix} \dot{\phi}_L \\ \dot{\phi}_R \end{pmatrix} \quad \Rightarrow \begin{pmatrix} \dot{\phi}_L \\ \dot{\phi}_R \end{pmatrix} = \begin{pmatrix} 1/r_w/ & 1/r_w \\ 1/b & -1/b \end{pmatrix} \begin{pmatrix} v \\ \dot{\theta} \end{pmatrix} \tag{6.6}$$

The operator station sends v and $\dot{\theta}$ as the command over the communication network to the robot. Therefore

$$\begin{pmatrix} u_r(t) \\ u_1(t) \end{pmatrix} = \begin{pmatrix} 1/r_w/ & 1/r_w \\ 1/b & -1/b \end{pmatrix} \begin{pmatrix} v \\ \dot{\theta} \end{pmatrix} \tag{6.7}$$

6.3 Simulation and Results

The teleoperation loop consists the operator model described in section 6.2 at one end of the communication link and Mobile robot model described in 6.1 on the other link. As shown in figure 6.4there will a delay in both direction of communication. In real system the video image is streamed by the robot. Due to large quantity of data and limited bandwidth the delay $h_1 >> h_2$. The amount of delay h_1 was measured and it was found around 0.5sec as described in appendix A. The command sent by the operator is v and $\dot{\theta}$ which is few bites only. Therefore in simulation $h_2 = 0$ is assumed.

6.3.1 The Simulation Algorithm

- Convert the path from global coordinate system (CS) to Robot Local CS
- With a given look ahead distance (l) search for a point on the path
  - If point is found goto step 3
  - If not found increase look ahead distance
- Determine the turning radius (r) using eqnation 6.5

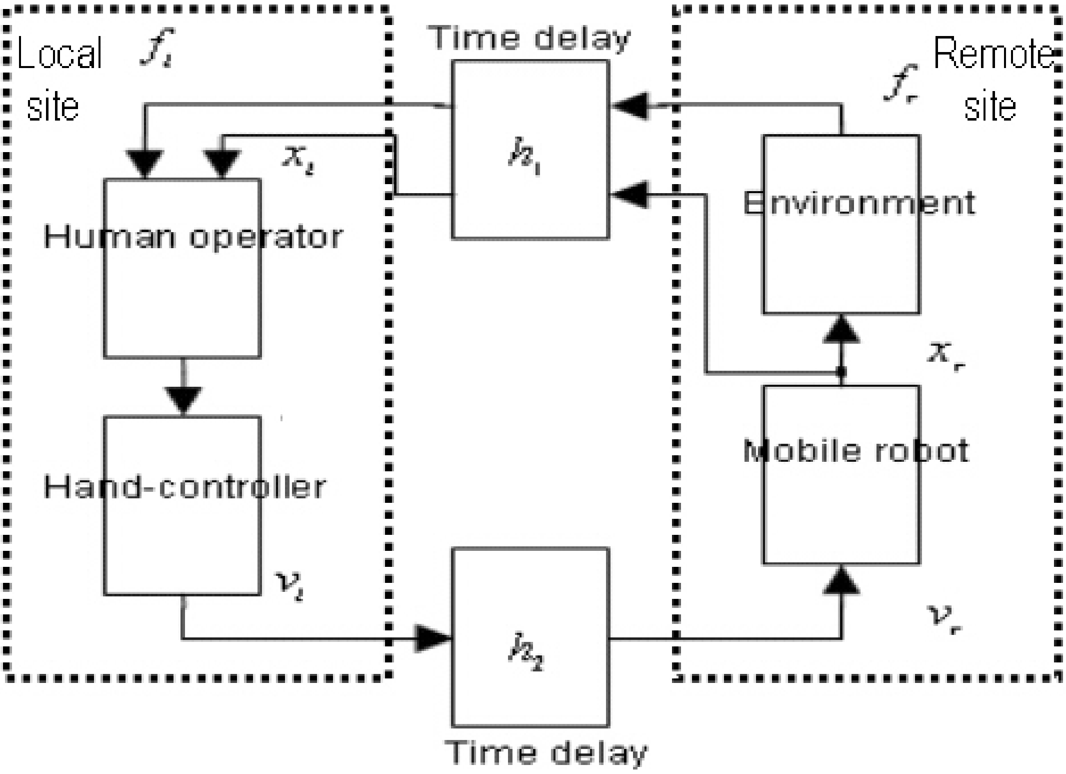
Local site
f_l
Time delay
h_1
Remote site
f_r
x_l
Human operator
Environment
x_r
Hand-controller
Mobile robot
v_l
h_2
v_r
Time delay

Figure 6.4: Teleoperation block diagram

- Calculate the command to the robot from equation 6.7. Note that these commands are based on the old visual data the operator see.
- Solve delayed differential equation in Matlab using *dde24*.

Simulation was carried using Matlab. Delay differential equation solver dde24 was used to solve equation 6.1 and 6.2 with delayed inputs u_r and u_l. The path tracked was a circle of radius 5m centred at origin of the global coordinate system. The human action was modelled with look ahead distance of 0.5m and linear velocity of 0.5m/s. The initial position of the robot was (4.5,0.0).

The performance of the system with zero delay, i.e. $h_1 = h_2 = 0$ is shown in figure 6.5. Figure 6.6 and 6.7 shows the plot robot motion under delay of 0.5 and 0.8 sec. It is seen that oscillation becomes visible at 0.5sec delay and with 0.8 sec delay the system is on the verge of instability.

It was also observed that the with large vehicle velocity, v and large look ahead distance, l the instability commences with smaller time delay, δ in equation 6.2.

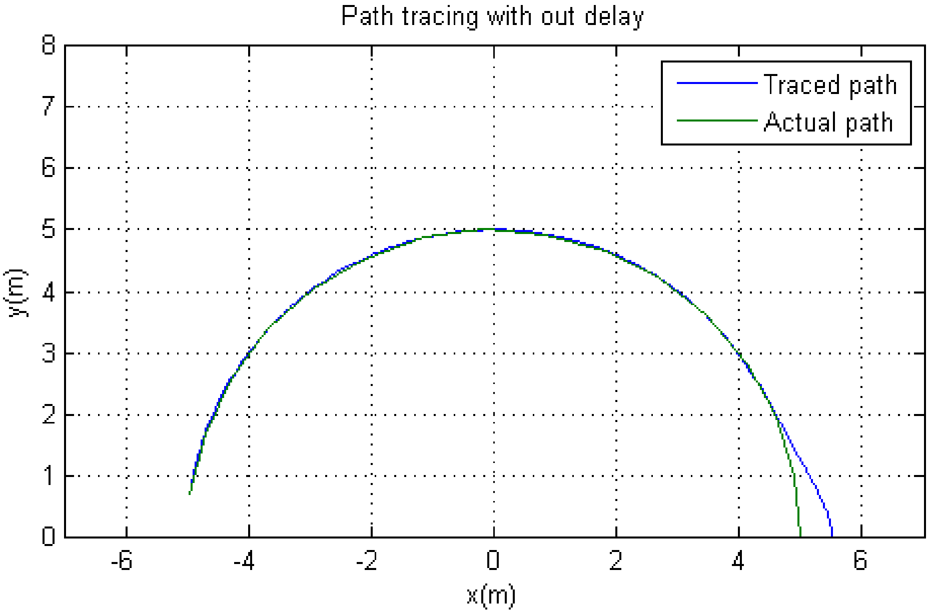

Figure 6.5: Simulation with no time delay in either direction

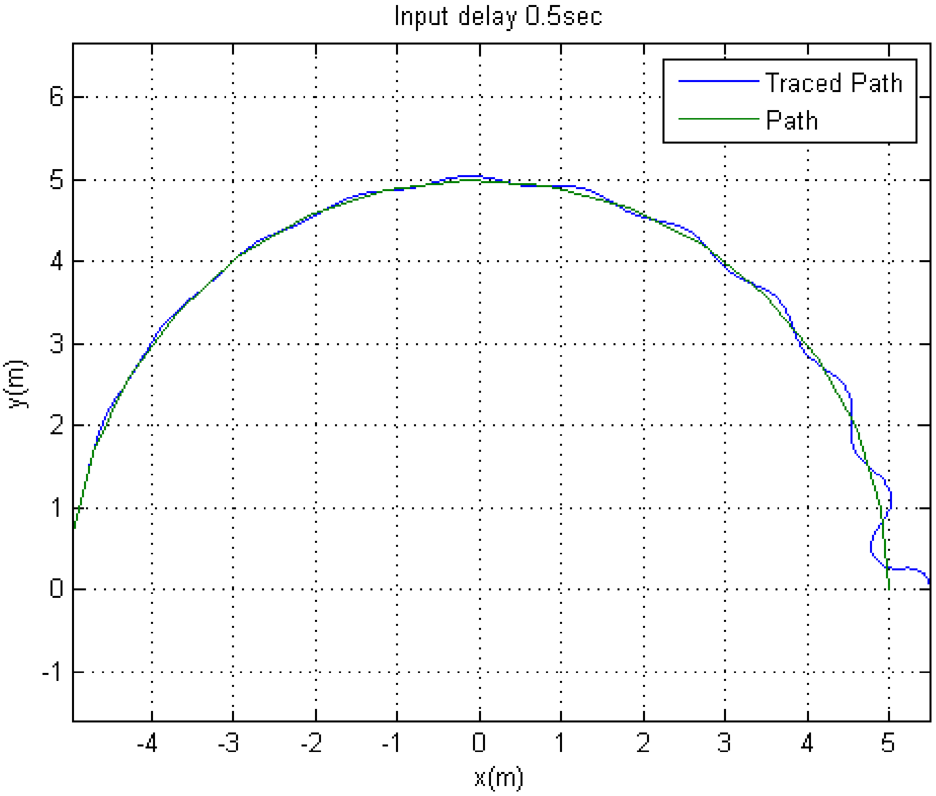

Figure 6.6: Simulation with time delay $h_1 = .5sec$ and $h_2 = 0$

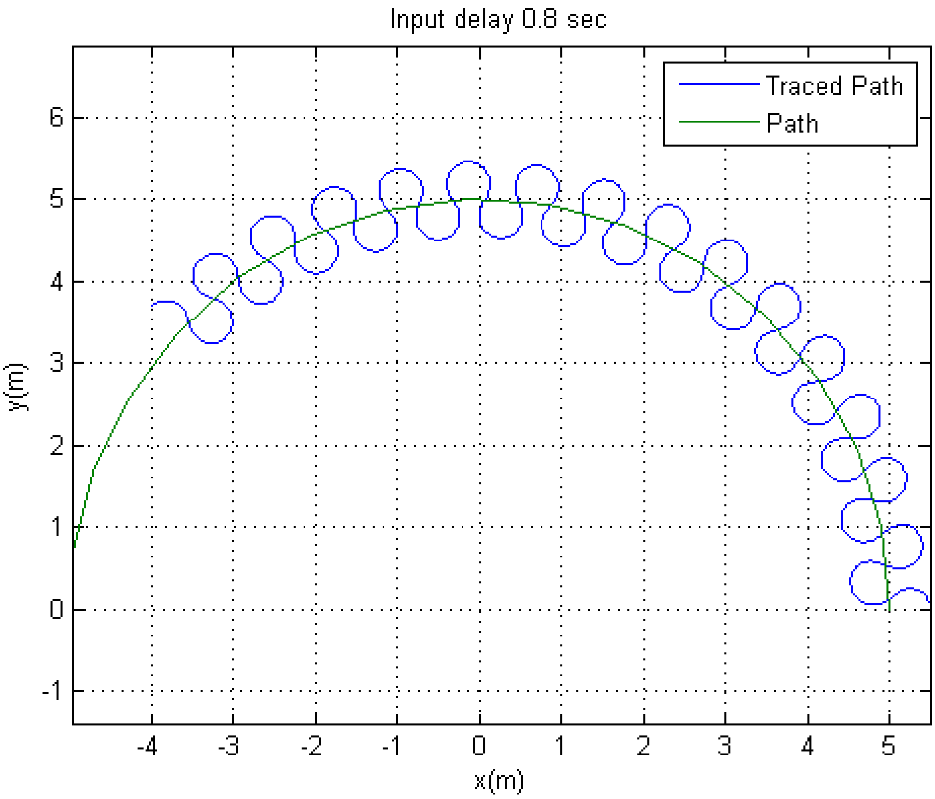

Figure 6.7: Simulation with time delay $h_1 = .8sec$ and $h_2 = 0$

6.4 Summary

In this chapter, simulation study of a teleoperated mobile robot was presented. A mathematical model was presented of the human operator action while driving the robot base on visual feed back. It was shown in by the simulation results that the behaviour of the system deteriorates with increase in delay in communication between the local and remote station. With large time delay the system becomes unstable.

In the next section we propose a predictive model based feedback control which is used to stabilize robot motion under time delay teleopration.

Chapter 7

Predictive Display

In the last chapter it was shown using simulation results that time delay between the remote and local station leads the system towards in stability. In this chapter we use predictive display to alleviate the above problem.

Predictive display has been defined as using the computer for extrapolating the display forward in time [31]. In this a local model of the remote scene is used to predict and render the remote scene in response to operator command. It replaces the delayed video feedback with extrapolated synthesised image of the remote environment and local enables the operator to perform the task normally.

7.1 Remote Scene Extrapolation

The visual data present in the current frame is the view that the robot has seen h_1 second earlier. In order to predict the current scene that the robot might be seeing we need to estimate the current position of the robot. Once the current position of the robot is known we re-construct a view form the old scene by moving the view point to the current position of the robot. To explain this further and to use it in the teleoperation simulation model discussed in chapter 6

7.1.1 here

Chapter 8

Conclusions

This chapter includes the thesis summary, major contributions and future scope of the work.

8.1 Thesis Summary

8.2 Future Scope of the work

The thesis opens up the following future directions:

(i) The

(ii) The

(iii) The

(iv) Implementing

Bibliography

[1] Y. Yamamoto and X. Yun, “Coordinating locomotion and manipulation of a mobile manipulator,” in *Decision and Control, 1992., Proceedings of the 31st IEEE Conference on*, pp. 2643–2648, IEEE, 1992.

[2] S. Rajendran and et.al., “Mobile robot for reactor vessel inspection,” in *National Conference on Advanced Manufacturing and Robotics*, pp. 2527–2532, CMERI, Durgapur,WB,, 2004.

[3] S. K. Saha and J. Angeles, “Kinematics and dynamics of a three-wheeled 2-dof agv,” in *Robotics and Automation, 1989. Proceedings., 1989 IEEE International Conference on*, pp. 1572–1577, IEEE, 1989.

[4] F. G. Pin and S. M. Killough, “A new family of omnidirectional and holonomic wheeled platforms for mobile robots,” *IEEE transactions on robotics and automation*, vol. 10, no. 4, pp. 480–489, 1994.

[5] J. E. M. Salih, M. Rizon, S. Yaacob, A. H. Adom, and M. R. Mamat, “Designing omni-directional mobile robot with mecanum wheel,” *American Journal of Applied Sciences*, vol. 3, no. 5, pp. 1831–1835, 2006.

[6] J. Suthakorn, S. S. H. Shah, S. Jantarajit, W. Onprasert, W. Saensupo, S. Saeung, S. Nakdhamabhorn, V. Sa-Ing, and S. Reaungamornrat, “On the design and development of a rough terrain robot for rescue missions,” in *Robotics and Biomimetics, 2008. ROBIO 2008. IEEE International Conference on*, pp. 1830–1835, IEEE, 2009.

[7] M. Guarnieri, R. Debenest, T. Inoh, E. Fukushima, and S. Hirose, “Development of helios vii: an arm-equipped tracked vehicle for search and rescue operations,” in *Intelligent Robots and Systems, 2004.(IROS 2004). Proceedings. 2004 IEEE/RSJ International Conference on*, vol. 1, pp. 39–45, IEEE, 2004.

[8] K. Nagatani, S. Tachibana, M. Sofne, and Y. Tanaka, “Improvement of odometry for omnidirectional vehicle using optical flow information,” in *Intelligent Robots and Systems, 2000.(IROS 2000). Proceedings. 2000 IEEE/RSJ International Conference on*, vol. 1, pp. 468–473, IEEE, 2000.

[9] J. Y. Wong, *Theory of ground vehicles*. John Wiley & Sons, 2008.

[10] T. Bevan, *Theory of Machines, Third Edition*. Delhi, India: CBS Publishers & Distributors, 1984.

[11] *Motor catalogue 2014*. Switzerland: Maxon Motors, 2017.

[12] J. T. Machado and M. F. Silva, “An overview of legged robots,” in *International symposium on mathematical methods in engineering*, MME Press Ankara, Turkey, 2006.

[13] K. P. Valavanis and G. J. Vachtsevanos, *Handbook of unmanned aerial vehicles*. Springer Publishing Company, Incorporated, 2014.

[14] J.-B. Mouret, *Evolutionary Adaptation in Natural and Artificial Systems*. PhD thesis, Université Pierre et Marie Curie, 2015.

[15] G. Campion, G. Bastin, and B. Dandrea-Novel, “Structural properties and classification of kinematic and dynamic models of wheeled mobile robots,” *IEEE transactions on robotics and automation*, vol. 12, no. 1, pp. 47–62, 1996.

[16] G. Campion and W. Chung, “Wheeled robots,” in *Springer Handbook of Robotics*, pp. 391–410, Springer, 2008.

[17] R. M. DeSantis, “Modeling and path-tracking control of a mobile wheeled robot with a differential drive,” *Robotica*, vol. 13, no. 04, pp. 401–410, 1995.

[18] K. C. Koh and H. S. Cho, “A smooth path tracking algorithm for wheeled mobile robots with dynamic constraints,” *Journal of intelligent & robotic systems*, vol. 24, no. 4, pp. 367–385, 1999.

[19] B. d’Andréa Novel, G. Campion, and G. Bastin, “Control of nonholonomic wheeled mobile robots by state feedback linearization,” *The International journal of robotics research*, vol. 14, no. 6, pp. 543–559, 1995.

[20] B. d’Andrea Novel, G. Bastin, and G. Campion, “Modelling and control of non-holonomic wheeled mobile robots,” in *Robotics and Automation, 1991. Proceedings., 1991 IEEE International Conference on*, pp. 1130–1135, IEEE, 1991.

[21] K. Thanjavur and R. Rajagopalan, “Ease of dynamic modelling of wheeled mobile robots (wmrs) using kane’s approach,” in *Robotics and Automation, 1997. Proceedings., 1997 IEEE International Conference on*, vol. 4, pp. 2926–2931, IEEE, 1997.

[22] S. K. Saha and J. Angeles, “Dynamics of nonholonomic mechanical systems using a natural orthogonal complement,” *Journal of Applied Mechanics*, vol. 58, no. 1, pp. 238–243, 1991.

[23] J. Angeles, *Fundamentals of robotic mechanical systems: theory, methods, and algorithms*, vol. 124. Springer Science & Business Media, 2013.

[24] S. Saha, *Introduction to robotics*. Tata McGraw-Hill, New Delhi, 2010.

[25] *EPOS Application Note: RS232 to CANopen Getway*. Maxon Motors, 2012.

[26] I. Farkhatdinov and J.-H. Ryu, "Hybrid position-position and position-speed command strategy for the bilateral teleoperation of a mobile robot," in *Control, Automation and Systems, 2007. ICCAS'07. International Conference on*, pp. 2442–2447, IEEE, 2007.

[27] M. Z. Zeroual, "maxon auto tuning," *iNaCoMM2013,IIT Roorkee, India*, 2013.

[28] *EPOS4 Application Note: Positioning Controllers.* Maxon Motors, 2012.

[29] J. Y. Chen, E. C. Haas, and M. J. Barnes, "Human performance issues and user interface design for teleoperated robots," *IEEE Transactions on Systems, Man, and Cybernetics, Part C (Applications and Reviews)*, vol. 37, no. 6, pp. 1231–1245, 2007.

[30] R. C. Coulter, "Implementation of the pure pursuit path tracking algorithm," tech. rep., Carnegie-Mellon UNIV Pittsburgh PA Robotics INST, 1992.

[31] S. T. B, "Space teleoperation through time delay: review and prognosis," *IEEE Transactions on Robotics and Automation*, vol. 9, no. 5, October 1993.

Appendix A

Simulation Time Delay Tele-operation

A.1 Measurment of Time Delay in Video Feedback

The experimental method used to find the delay in video stream coming from the remote station is described here.

Appendix B

Dynamics

B.1 Inertia Dyad

The dyadic product takes two vector and returns a second-order tensor. If **a** and **b** are two vectors expressed as $\mathbf{a} \equiv a_1\mathbf{i} + a_2\mathbf{j} + a_3\mathbf{k}$ and $\mathbf{b} \equiv b_1\mathbf{i} + b_2\mathbf{j} + b_3\mathbf{k}$. Then the dyadic product of **a** and **b** are defined as:

Publications from the Thesis

Research papers published/presented/under preparation are listed below

1. Hayat, A.A., Abhishek, V., Saha, S.K., Dynamic Identification of Manipulator: Comparison between CAD and Actual Parameters, 17*th National and 2nd International Conference on Machine and Mechanisms, iNaCoMM 2015*, IIT Kanpur, Dec. 16–19, 2015.
2. Udai, A. D., Hayat, A. A., Saha, S. K., “Parallel Active/Passive Force Control of Industrial Robots with Joint Compliance,” *IEEE/RSJ International Conference on Intelligent Robots and Systems (IROS 2014), Chicago, Illinois*, Sept. 14–18 , 2014.

Brief Bio-data of the Author